

Cement and Concrete Composites

Tensile behavior of rebar-reinforced coarse aggregate ultra-high performance concrete (R-CA-UHPC) members: Experiments and restrained shrinkage creep effect --Manuscript Draft--

Manuscript Number:	CCC-D-24-00270
Article Type:	Research Paper
Keywords:	UHPC members; axial tensile response; Restrained Shrinkage; tensile creep; first cracking strength
Corresponding Author:	Qingtian Su, Ph.D. Tongji University Shanghai, Shanghai CHINA
First Author:	Zhanchong Shi
Order of Authors:	Zhanchong Shi Minfei Liang Qingtian Su Terje Kanstad Liberato Ferrara
Abstract:	<p>Rebar-reinforced coarse aggregate ultra-high-performance concrete (R-CA-UHPC) has been used in the construction of new structures and strengthening of deteriorated aged infrastructures, and it inevitably sustains tension. To study the tensile behavior of R-CA-UHPC members, axial tensile tests for dog-bone-shaped specimens were designed and conducted. The investigated variables included reinforcement ratio in terms of rebar quantity /diameter, and concrete type (CA-UHPC vs. normal concrete). The test results showed that the improved rebar/CA-UHPC bond property prevents the emergence of splitting cracks, but intensifies the crack localization for CA-UHPC and strain concentration for rebar after yielding. Moreover, the restrained effect of rebar on free shrinkage of CA-UHPC leads to a decrease in the first cracking strength for R-CA-UHPC members. Based on the established development functions of elastic modulus, autogenous shrinkage, and tensile creep for CA-UHPC, the restrained effect was quantified according to Dischinger's-differential-equation-based theoretical analysis. Finally, the models to predict the first cracking stress/strain and the yielding load of the R-CA-UHPC members were developed and validated.</p>
Suggested Reviewers:	<p>Eugen Brühwiler, PhD Head of Laboratory of Maintenance and Safety of Structures, Swiss Federal Institute of Technology Lausanne eugen.bruehwiler@epfl.ch Prof. Eugen Brühwiler is a leading expert in ultra-high-performance concrete</p> <p>Viktor Mechtcherine, PhD Institute Director of Institute of Concrete Materials, TU Dresden viktor.mechtcherine@tu-dresden.de Prof. Viktor Mechtcherine is a leading expert in fiber-reinforced cementitious composites</p> <p>Doo-Yeol Yoo, PhD Yonsei University dyyoo@yonsei.ac.kr Doo-Yeol Yoo is a leading expert in shrinkage behavior of fiber-reinforced cementitious composite</p>

Tensile behavior of rebar-reinforced coarse aggregate ultra-high-performance concrete (R-CA-UHPC) members: Experiments and restrained shrinkage creep effect

By **Zhanchong Shi, Minfei Liang, Qingtian Su, Terje Kanstad, and Liberato Ferrara**

The authors wish to sincerely thank the editor of the Cement and Concrete Composites for the consideration given to this paper. We believe that this article is in line with the aims of the journal, since it presents information pertaining to the tensile behaviour of rebar-reinforced coarse aggregate ultra-high-performance fiber-reinforced concrete (R-CA-UHPC).

CA-UHPC is an advanced fiber-reinforced cementitious composites used in the strengthening and retrofitting application of deteriorated infrastructures, such as bridges, tunnels, and roads. In this paper, the axial tensile test of R-CA-UHPC elements was designed and conducted. The tensile response and failure modes of R-CA-UHPC elements were revealed. The restrained effect of rebar on free shrinkage of CA-UHPC at curing stage was quantified based on test results and theoretical analysis. Finally, the restraint degree and free degree were proposed to evaluate the restrained effect. Base on this, the models to predict the first cracking strength/strain and yielding load of R-CA-UHPC elements were developed and validated by comparison with test results.

This paper bridges the gap between the tensile properties of CA-UHPC material and the tensile performance of R-CA-UHPC structure, i.e. the tensile behavior characterization at the R-CA-UHPC member level.

Yours sincerely,

Zhanchong Shi

Minfei Liang

Qingtian Su

Terje Kanstad

Liberato Ferrara

- Comparison of the tensile response differences between R-NC and R-CA-UHPC members
- Discovery of the influence of restrained effect on decrease of the first-cracking strength
- Establishment of the development functions of elastic modulus, autogenous shrinkage, and tensile creep for CA-UHPC at early age
- Proposition of restraint/free degree and development of their relations with axial stiffness ratio
- Establishment and validation of prediction models of the first-cracking strength/strain and yield load for R-CA-UHPC members

Title page

Title: Tensile behavior of rebar-reinforced coarse aggregate ultra-high performance concrete (R-CA-UHPC) members: Experiments and restrained shrinkage creep effect

Author names: Zhanchong Shi^{a,b}, Minfei Liang^c, Qingtian Su^{a,d,*}, Terje Kanstad^b, Liberato Ferrara^e

Affiliations: ^aDepartment of Bridge Engineering, Tongji University, Shanghai 200092, China;

^bDepartment of Structural Engineering, Norwegian University of Science and Technology, Richard Birkelandsvei 1A, 7034 Trondheim, Norway

^cMicrolab, Delft University of Technology, 2628CN Delft, The Netherlands

^dShanghai Engineering Research Center of High Performance Composite Bridges, Shanghai 200092, China;

^eDepartment of Civil and Environmental Engineering, Politecnico di Milano, Piazza Leonardo DaVinci 32, 20133 Milan, Italy

Corresponding author: Qingtian Su (E-mail: sqt@tongji.edu.cn)

Address: 1239 Siping Road, Tongji University, Shanghai 200092, China

37 cross-sectional area, and has been used in rehabilitation and strengthening of aged
38 infrastructures, such as deteriorated concrete slabs and beams [2–5] and fatigue-cracked
39 orthotropic steel bridge decks [6–8]. Whereas, the use of an extremely low water-binder (w/b)
40 ratio of less than 0.2 and a substantial amount of binder of typically 800–1200 kg/m³ make
41 UHPC have a significantly higher autogenous shrinkage compared to normal concrete and
42 high-performance concrete [9]. To address this issue, one solution is to introduce coarse
43 aggregate (CA) to partially replace binders in UHPC, obtaining what is also known as coarse
44 aggregate UHPC (CA-UHPC), because the stiff and high elastic modulus of CA contributes to
45 restraining shrinkage deformation of UHPC [10]. It has been demonstrated that, with the
46 appropriate addition of coarse aggregates, CA-UHPC features higher compressive strength
47 and elastic modulus and a slight decrease in tensile capacity and post-cracking toughness, as
48 compared with “conventional” UHPC mixes (with the same paste ratio) with only (very) fine
49 aggregates [11,12].

50 Though exhibiting a slightly deteriorated tensile behavior, CA-UHPC is expected to be
51 co-reinforced with steel rebars and employed in tension zones of concrete structures. Current
52 research on the tensile properties of CA-UHPC mainly focuses on the material level. Shi et al.
53 [13] have developed the tensile constitutive model and tensile damage evolution law for CA-
54 UHPC based on quasi-static uniaxial tensile tests, demonstrating that CA-UHPC exhibits
55 approximately linear-elastic response up to tensile strength followed by tension softening. Li
56 et al. [14] conducted uniaxial tensile fatigue test and 3D numerical simulation for CA-UHPC
57 with different volume additions of CA, revealing that CA weakens the fatigue deformation
58 capacity and accelerates the initiation of tensile fatigue damage at the early stage, resulting in
59 premature fatigue failure. Cheng [15] established the flexural tensile fatigue *S-N* curves with
60 different survival probabilities for CA-UHPC based on four-point bending cyclic tests. As for
61 the tensile behavior of CA-UHPC at the structural level, quasi-static flexural [16,17] as well
62 as the fatigue flexural tests [18,19] have been performed on rebar-reinforced CA-UHPC (R-
63 CA-UHPC) bridge decks to reveal the flexural response and fatigue resistance. However, to
64 the authors’ knowledge, there is currently no study on the axial tensile behavior of R-CA-
65 UHPC elements at the member level. The axial tensile behavior of R-CA-UHPC members
66 better reflects the synergistic tensile response of rebar and CA-UHPC compared to the
67 flexural performance of R-CA-UHPC members or structures.

68 Recent studies on axial tensile behavior of rebar-reinforced UHPC (R-UHPC) members
69 mainly employed UHPC without CA, and focused on the influences of material parameters,
70 including reinforcement ratio, rebar type (plain and ribbed rebars, normal and high strength
71 rebars), fiber volume fraction, fiber distribution, and fiber chemical treatment, on the tensile
72 response [20–31]. Overall, the consistent conclusion that UHPC contributes a substantial
73 tensile capacity to the member response even after rebar yields, can be drawn. However, only
74 Yuan [23], Bian et al. [26,28], and Guo et al. [27] reported that the first cracking strength of
75 the R-UHPC member is significantly lower than the elastic tensile strength of the “parent”
76 UHPC material, and this difference increases with the growing reinforcement ratio. This can
77 be interpreted by the restrained effect of rebar on the free shrinkage of UHPC.

78 Past research regarding the cracking of restrained concrete [32,33], including internal

79 restraint (such as rebar) as well as external restraint (such as boundary conditions), has
80 demonstrated that restrained shrinkage leads to tensile stress which may result in even
81 premature cracking in concrete. Whereas the tensile creep partially counteracts the tensile
82 stress in concrete through a stress relaxation mechanism. Whether the significantly high
83 autogenous shrinkage of UHPC will induce, if restrained, tensile stresses even more
84 prominent in R-UHPC members before external loading deserves to be investigated. What's
85 more, the influence of the restrained shrinkage on the first cracking strength of R-UHPC
86 members hasn't been quantified. Moreover, whether the axile tensile response of R-UHPC
87 members is suitable for R-CA-UHPC members is thus to be investigated further.

88 Consequently, this study mainly focuses on the axial tensile behavior of R-CA-UHPC
89 members based on the quasi-static axial tensile test, and the influence of reinforcement ratios
90 and concrete types was investigated. This paper compares the global tensile response,
91 cracking patterns, and ultimate failure modes between R-CA-UHPC and rebar-reinforced
92 normal concrete (R-NC) members. The influence of restrained shrinkage and tensile creep on
93 the restrained tensile stress at the curing stage was quantified according to Dischinger-
94 differential-equation-based theoretical analysis. On this basis, concepts of restraint degree and
95 free degree were proposed to characterize the restrained shrinkage creep effect, and prediction
96 models for the first cracking strength/strain and the yielding load for R-CA-UHPC members
97 were developed and validated.

98 **2. Research significance**

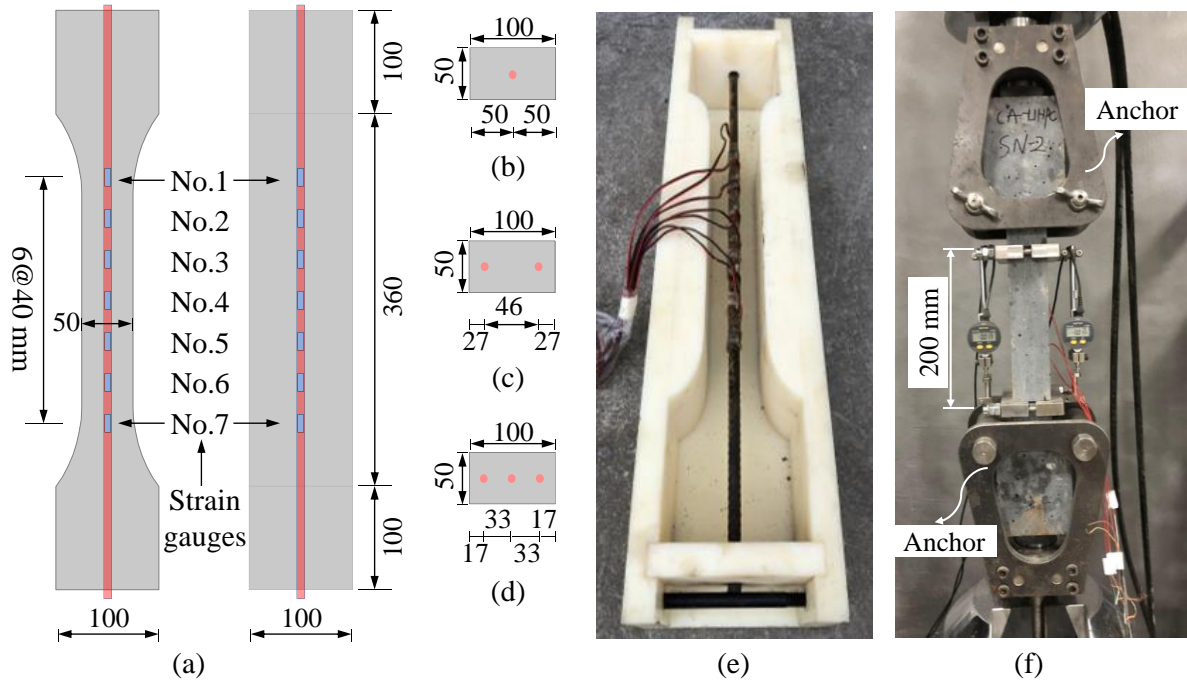
99 The axial tensile behavior of R-CA-UHPC members is fundamental research for RC
100 structures, which will bridge the gap of CA-UHPC between the material level and the
101 structural level, i.e., the member level. It will open our understanding of the synergetic tensile
102 property of rebar and CA-UHPC, and the influence of the restrained shrinkage creep effect for
103 R-UHPC members. The results are useful to characterize and model the mechanical behavior
104 of R-CA-UHPC members and to make predictions of the first cracking strength/strain and the
105 yielding load for engineers.

106 **3. Experimental program**

107 *3.1 Specimen design and production*

108 Dog-bone-shaped reinforced concrete specimens, as shown in Fig.1, were designed to
109 conduct the axial tensile test. The specimens were 100 mm thick and 560 mm long, with a
110 cross-section 50 mm wide in the central part, which tapered to 100 mm at the edges. To
111 quantify the synergistic tensile property of rebar and CA-UHPC elements, and to compare the
112 difference in the tensile response between R-CA-UHPC members and rebar-reinforced normal
113 concrete (R-NC) members, three parameters were assumed as experimental variables: (a) the
114 reinforcement ratio, equal to 1.6%, 3.2%, and 5.0%, obtained with one, two or three 10 mm
115 diameter bars respectively; (b) the bar diameter d_s , equal to 10 mm, 12 mm, 14 mm, and 16
116 mm with one single rebar, corresponding to reinforcement ratio of 1.6%, 2.3%, 3.2%, and
117 4.2%, respectively, (c) concrete type, either CA-UHPC or NC. Table 1 provides a synopsis of

118 the experimental variables and program.



119
120 **Fig. 1.** Specimen details (unit: mm): (a) sample size and arrangement of rebar strain gauges;
121 (b) cross section with single rebar; (c) cross section with two rebars; (d) cross section with
122 three rebars; (e) specimen mold; (f) axial tensile test setup.

123
124 **Table 1.** Specimen details of reinforced concrete.

Rebar configuration	ρ_s	c [mm]	Specimen number	Concrete type
d_s10	1.6%	20	SN-1~SN-5	CA-UHPC
$2d_s10$	3.2%	20	SN-1~SN-5	CA-UHPC
$3d_s10$	5.0%	12	SN-1~SN-5	CA-UHPC
d_s12	2.3%	19	SN-1~SN-5	CA-UHPC
d_s14	3.2%	18	SN-1~SN-5	CA-UHPC
d_s16	4.2%	17	SN-1~SN-5	CA-UHPC
d_s12	2.3%	19	SN-1~SN-5	NC

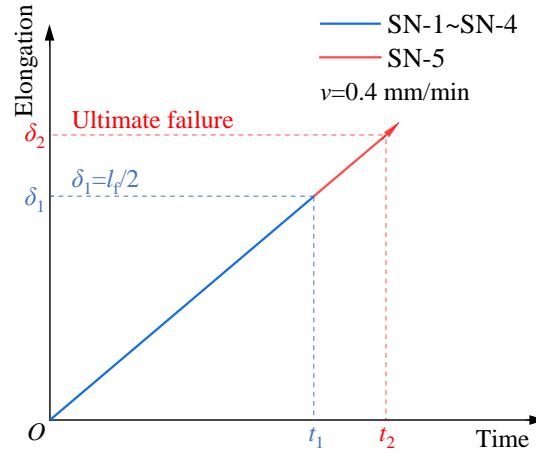
125 Notes: ρ_s , c denote reinforcement ratio and minimum concrete cover, respectively.

126 For each combination of experimental variables, five nominally identical samples
127 numbered SN-1 to SN-5 were produced. Seven strain gauges (8 mm long and 5 mm wide)
128 with uniform spacing of 40 mm, shown in Fig.1(a) and Fig.1(e), were attached to the rebar
129 surface (embedded in concrete) only for specimens SN-3 and SN-4 to measure the strain
130 distribution along the bars; it is worth remarking that the first cracking load may be affected
131 by the increased reduction of cross-section induced by the wires of strain gauges. Only one
132 rebar was provided with strain gauges for the specimen with two rebars, while only the
133 middle rebar was equipped with strain gauges for the specimen with three rebars.

134 The casting process of the specimens was as follows: first, the rebars were fixed at the
135 specimen mold, shown in Fig.1(e), then the fresh concrete mixture was cast into the mold
136 which was vibrated for 2-3 minutes afterward. The specimens were covered with plastic film
137 immediately after vibration to prevent moisture evaporation. Finally, the specimens were
138 demolded 24 hours (at room temperature of $20 \pm 2^\circ\text{C}$) after casting and cured for 28 days at the

139 standard curing room with a temperature of $20\pm 2^\circ\text{C}$ and a relative humidity of 95%.

140 3.2 Test setup and loading protocol



141
142 **Fig. 2.** Loading protocol.

143 Fig.1(f) shows the axial tensile test setup. A servo-hydraulic testing machine was used to
144 enforce direct tensile load to the specimen under constant displacement control at a rate of 0.4
145 mm/min. Two extensometers with an accuracy of 0.001 mm were attached to the central part
146 (longitudinal direction) of the specimen over a gauge length of 200 mm to measure the axial
147 elongation. The opening of the cracks within the gauge length was captured by a crack
148 observation instrument with an accuracy of 0.01 mm. In addition, the strain evolution along
149 the rebar was recorded by strain gauges and the DH3816N static data acquisition instrument.
150 As shown in Fig.2, specimens SN-1~SN-4 were loaded to a maximum elongation of 6.5 mm
151 (half of the steel fiber length l_f , $l_f = 13$ mm) and unloaded, while specimens SN-5 were loaded
152 to the ultimate failure.

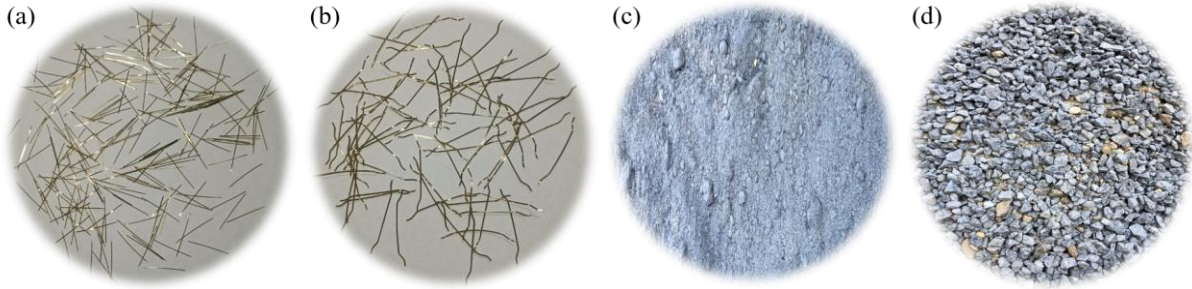
153 3.3 Material properties characterization

154 3.3.1 Concrete

155 The two concrete materials used were commercial ones. CA-UHPC was composed of
156 reactive powder, river sand, basalt aggregate (maximum particle size less than 8 mm),
157 superplasticizer, water, and steel fibers, as shown in Fig.3 and Table 2. The steel fibers were a
158 fiber cocktail containing straight fibers (length of 13 mm and diameter of 0.2 mm) as well as
159 hooked-end fibers (length of 20 mm and diameter of 0.25 mm). The total fiber dosage was
160 2.5% by volume (1% of straight fibers and 1.5% of hooked-end ones). The elastic modulus
161 and tensile strength of the two steel fibers were 200 GPa and 2850 MPa, respectively. NC did
162 not contain steel fibers, and the composition of NC is listed in Table 3.

163 Axial tensile tests were conducted on the investigated CA-UHPC and NC (unreinforced)
164 using the same dog-bone-shaped specimens as for the R-CA-UHPC/RC to identify the tensile
165 constitutive relationship. Referring to Chinese Standard CECS13 [34], $100\text{ mm} \times 100\text{ mm} \times$
166 300 mm prisms for CA-UHPC and $150\text{ mm} \times 150\text{ mm} \times 300\text{ mm}$ ones for NC, were used to
167 obtain the elastic modulus and axial compressive strength. Each test was performed on three
168 nominally identical specimens, and the corresponding average values and standard deviations
169 are summarized in Table 4. It should be noted that the casting process and curing condition of

170 the material property test specimens were the same as the reinforced concrete specimens
 171 mentioned above.



172
 173 **Fig. 3.** Main compositions of CA-UHPC: (a) straight steel fibers; (b) hooked-end steel fibers;
 174 (c) reactive powder; (d) basalt aggregates.

175 **Table 2.** Material compositions of 1 m³ CA-UHPC (unit: kg).

Reactive powder	Sand	Basalt aggregates	Steel fibers		Superplasticizer	Water
			straight	hooked		
1173	616	472	89	109	25.7	138

176 **Table 3.** Material compositions of 1 m³ NC (unit: kg).

Gravel	Sand	Cement	Water reducer	Water
1080	780	450	4.5	154

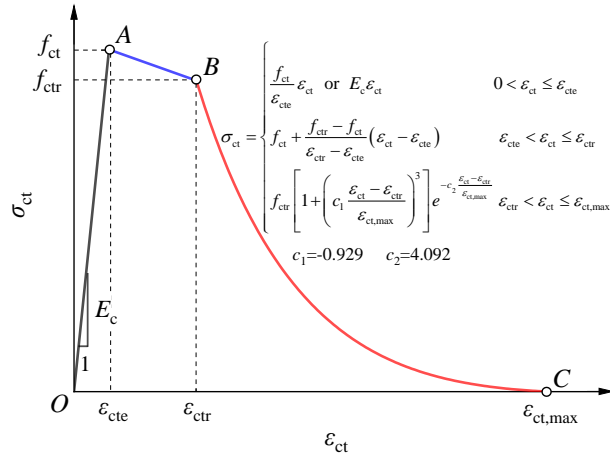
177 **Table 4.** Basic mechanical properties of investigated concretes

Concrete	E_c [MPa]	f_c [MPa]	f_{ct} [MPa]	f_{ctr} [MPa]	ϵ_{ctr} [$\times 10^{-6}$]	$\epsilon_{ct,max}$ [$\times 10^{-6}$]
CA-UHPC	52000±6538	128±10	7.83±0.78	6.47±0.84	2500	32500
NC	36633±3296	49±5	2.59±0.28	—	—	—

178 Notes: E_c and f_c denote elastic modulus and compressive strength, respectively. f_{ct} , f_{ctr} , ϵ_{ctr} , and $\epsilon_{ct,max}$ are the
 179 tensile strength, post-peak residual tensile strength, post-peak residual tensile strain, and maximum tensile
 180 strain, respectively.

181 According to the axial tensile results and the author's previous work [13], the direct
 182 tensile behavior of the CA-UHPC is characterized by an approximately linear stress-strain
 183 relation up to the peak stress (tensile strength) and the post-peak tensile softening response,
 184 which is mainly induced by the weak zone at the coarse-aggregate/matrix interface. Therefore,
 185 CA-UHPC was considered the strain-softening type according to the axial tensile response.
 186 The tensile constitutive model of CA-UHPC was established, plotted in Fig.4, and the
 187 corresponding characteristic parameters f_{ct} , f_{ctr} , ϵ_{ctr} , and $\epsilon_{ct,max}$ are listed in Table 4. As shown
 188 in Fig.4, the softening branch is divided into the multi-cracking stage (corresponding to
 189 branch AB) and the localized-cracking stage (corresponding to branch BC).

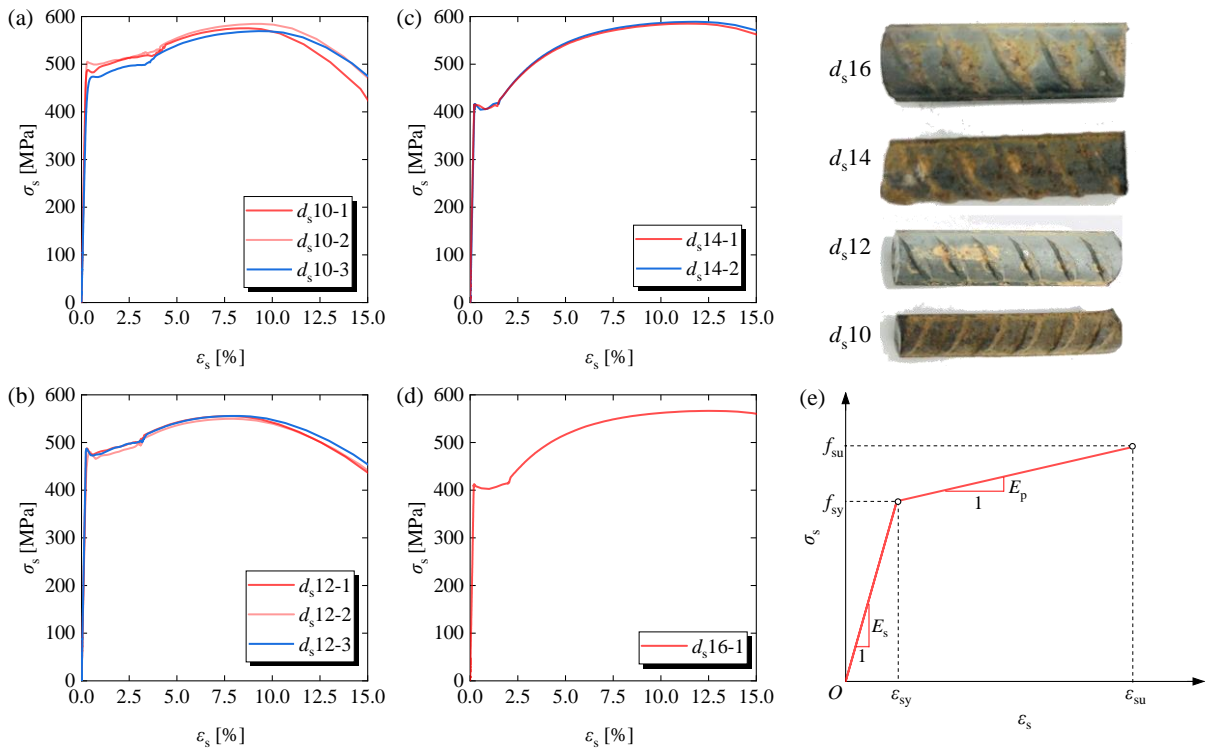
190



191
192 **Fig. 4.** Tensile constitutive model of CA-UHPC [13].

193 **3.3.2 Rebar**

194 The steel rebar used was HRB400 which is mostly used in concrete bridges in China.
195 Axial tensile tests on rebar samples (three per diameter) were performed according to the
196 Chinese standard [35], The obtained tensile stress-strain curves are shown in Fig.5(a)~(d). A
197 simplified bilinear constitutive model (Fig. 5(e)) was developed based on the tensile stress-
198 strain curves, and the characteristic parameters of the model are presented in Table 5. These
199 parameter values represented the average values obtained from the successfully tested
200 specimens in which fracture occurred within the gauge length of the extensometer.



201
202 **Fig. 5.** Tensile stress-strain curves of the rebar: (a) d_s 10 mm; (b) d_s 12 mm; (c) d_s 14 mm; (d)
203 d_s 16 mm; (e) simplified bilinear constitutive model.

206

Table 5. Characteristic parameters of the bilinear constitutive model for the steel rebar.

d_s [mm]	f_{sy} [MPa]	f_{su} [MPa]	ε_{sy} [$\times 10^{-6}$]	ε_{su} [$\times 10^{-6}$]	E_s [MPa]	E_p [MPa]
10	488	577	2438	90042	200187	1010
12	470	554	2382	77811	197439	1103
14	406	587	2104	116164	192978	1587
16	407	566	1958	124925	207880	1296

207

Notes: f_{sy} , f_{su} , ε_{sy} , ε_{su} , E_s , and E_p denote the yielding strength, tensile strength, yielding strain, tensile strain corresponding to the tensile strength, elastic modulus, and plastic modulus, respectively.

208

209

4. Test results and analysis

210

4.1 Axial load-member strain response

211

4.1.1 General axial tensile response

212

213

214

215

216

217

The axial load vs. average member strain response of the tested R-CA-UHPC and R-NC specimens is plotted in Fig.6. The average member strain was obtained by dividing the mean value of the elongations measured through the two extensometers by the gauge length of 200 mm. Fig.6 also compares the axial tensile response between the reinforced concrete member and the bare rebar, in which the bare rebar response was obtained using the bilinear constitutive model developed above.

218

219

220

221

222

223

224

225

226

227

228

As shown, the axial tensile response curve of the R-NC specimen is almost the same as that of the bare rebar, indicating that the NC provides limited tensile capacity to the R-NC members. By contrast, the axial tensile response curve of the R-CA-UHPC specimen lies evidently above the bare rebar curve, and the significant gap between the two curves stands for the CA-UHPC's contribution to the tensile bearing capacity of the R-CA-UHPC members. Specimens SN-1 and SN-2 always have excellent repeatability, while the tensile responses of specimens SN-3 and SN-4, in most cases (for d_s10 , $2d_s10$, $3d_s10$, and d_s12), are located below that of specimens SN-1 and SN-2, which can probably be due to some disturbance effects of the strain gauges, also on the flow of the CA-UHPC and hence on fiber dispersion. Therefore, the following analysis of axial load vs. average member strain will be mainly based on the test results of specimens SN-1 and SN-2.

229

230

231

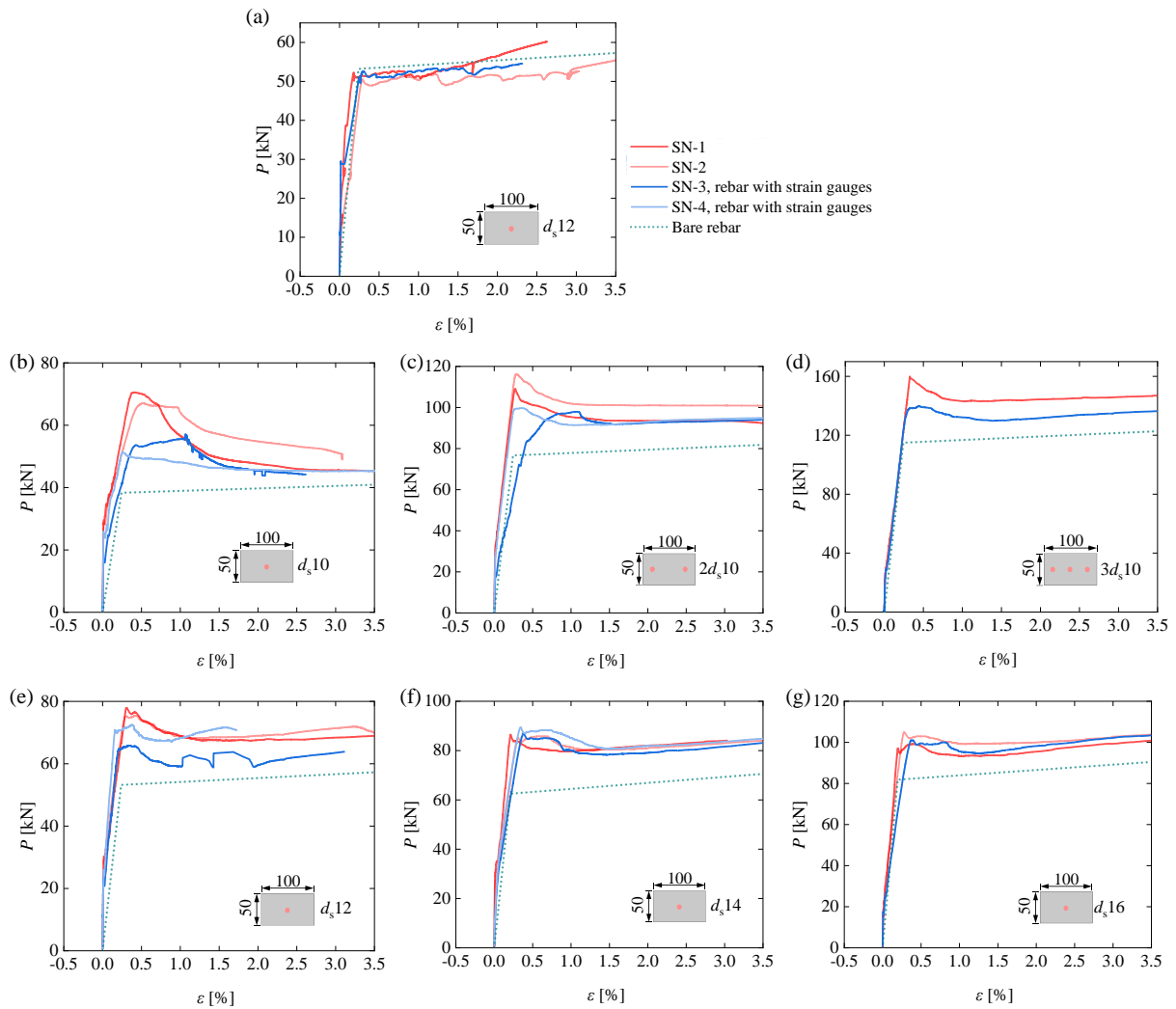
232

233

234

235

The representative axial tensile response, as from the tested R-NC/CA-UHPC members, is plotted in Fig.7. The first cracking point (ε_{cr} , P_{cr}) was determined by the initial shifting from the linear-elastic tensile response curve. The yielding point (ε_y , P_y) was obtained when the average member strain reached the yielding strain of the rebar listed in Table 5. The peak point (ε_m , P_m) was achieved as the axial load reached the maximum value. The fracture point (ε_f , P_f) indicated the moment the rebar was ruptured, and this point was identified based on the ultimate axial tensile response of specimen SN-5.

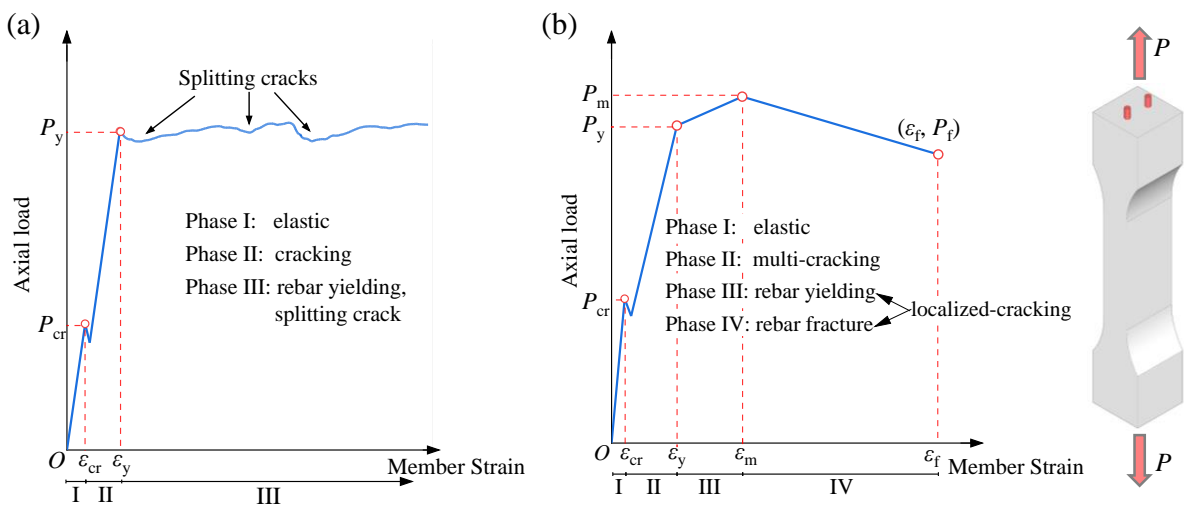


236

237 **Fig. 6.** Axial load-average member strain response of reinforced concrete members: (a) R-NC;

238 (b) R-CA-UHPC, d_s10 ; (c) R-CA-UHPC, $2d_s10$; (d) R-CA-UHPC, $3d_s10$; (e) R-CA-UHPC,

239 d_s12 ; (f) R-CA-UHPC, d_s14 ; (g) R-CA-UHPC, d_s16 .



240

241 **Fig. 7.** Schematic representative of the axial tensile response of reinforced concrete members:

242 (a) R-NC; (b) R-CA-UHPC.

243 As shown in Fig.7, the axial tensile response of R-NC members could be divided into
244 three phases.

245 Phase I: linear-elastic phase, featured by the linear axial load-average member strain
246 relation until NC reaches its tensile strength. The first cracking of NC marks the end the Phase
247 I.

248 Phase II: stabilized cracking phase. At this phase, the concrete at the cracked location
249 enters its softening stage, and the tensile force is transferred to the neighboring concrete that
250 has not yet cracked through the bond interaction between rebar and concrete. New transverse
251 cracks continue to appear in the concrete and develop into main cracks with a saturated
252 distribution until the rebar yields.

253 Phase III: yielding phase, characterized by the pronounced yielding plateau of the tensile
254 response curve; the formation of longitudinal splitting cracks along the rebar has been
255 observed in this stage, as a result of the failure of the bond mechanism, which can be reflected
256 by the unevenness at the yielding plateau shown in Fig.7(a). The splitting cracks continue to
257 propagate until they intersect with the transverse cracks, splitting the R-NC members into
258 several sub-components bounded by longitudinal and transverse cracks, presenting the
259 ultimate failure mode of "shattering to pieces", shown in sec. 4.4 below. It is noteworthy that
260 only rebar bears tension at the yielding phase.

261 By contrast, the axial tensile response of the R-CA-UHPC members could be divided
262 into four phases, including the linear-elastic phase, stabilized cracking phase, yielding phase,
263 and rebar fracture phase. The first three phases of the R-CA-UHPC members are generally the
264 same as the R-NC members, the differences are:

265 (a) The CA-UHPC at the cracked sections can still bear tension due to the fiber bridging
266 effect and the pull-out effect of debonding between the steel fibers and the matrix.

267 (b) Although new transverse cracks continue to appear for the R-CA-UHPC members at
268 the stabilized cracking phase (phase II in Fig7(b), corresponding to the multi-cracking
269 softening stage of CA-UHPC material as described in sec.3.3.1), only one transverse crack
270 develops into a localized main crack once reaching yielding (phases III and IV in Fig7(b),
271 corresponding to the localized-cracking softening stage of CA-UHPC material as described in
272 sec.3.3.1). Consequently, the rest transverse cracks are gradually closed because they can't be
273 captured by visual observation.

274 (c) No splitting cracks initiate for the R-CA-UHPC members at the yielding phase,
275 indicating that the higher tensile strength of CA-UHPC suppresses the occurrence of splitting
276 cracking. Moreover, the axial load continues to increase at this phase without a yielding
277 plateau, suggesting that the excellent interface bond property between rebar and CA-UHPC
278 ensures the synergy to withstand tension even after crack localization.

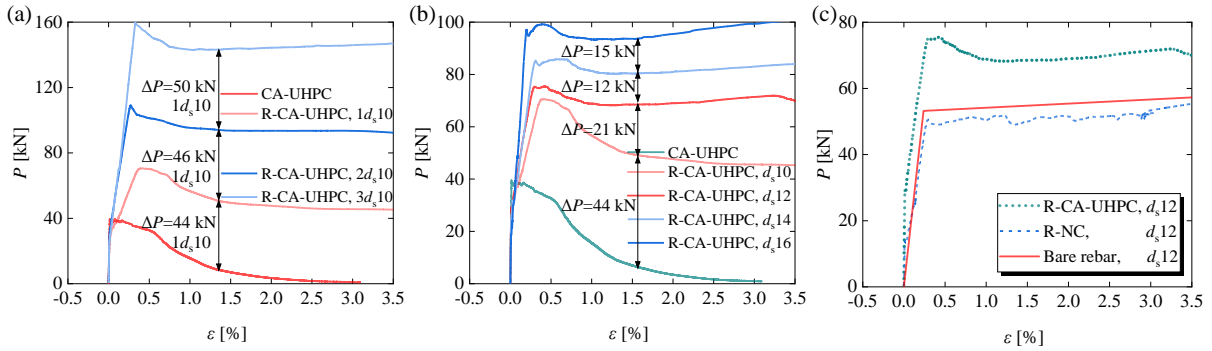
279 (d) After crossing the peak point, as the main crack continues to expand, the rebar at the
280 main crack location is broken while the two ends of the rebar are firmly anchored in CA-
281 UHPC, as shown in sec.4.4.

282 4.1.2 Influence of investigated parameters

283 The influence of investigated parameters, i.e., rebar quantity, rebar diameter, and

284 concrete type, on the axial tensile response of R-CA-UHPC members is shown in Fig.8. For
 285 rebar quantity, it is obvious that the load-bearing capacity exhibited a linear increment with
 286 the number of bars with the same diameter was increased from 0 to 3. Moreover, from the
 287 unreinforced member to R-CA-UHPC member with single rebar, two rebars, and three rebars,
 288 the residual tensile bearing capacity increases were 44 kN, 46 kN, and 50 kN, respectively.
 289 The increases were almost equal, which was equal to the yield-bearing capacity $f_{sy}A_s$ (A_s is the
 290 cross-sectional area of a single bar) of single rebar.

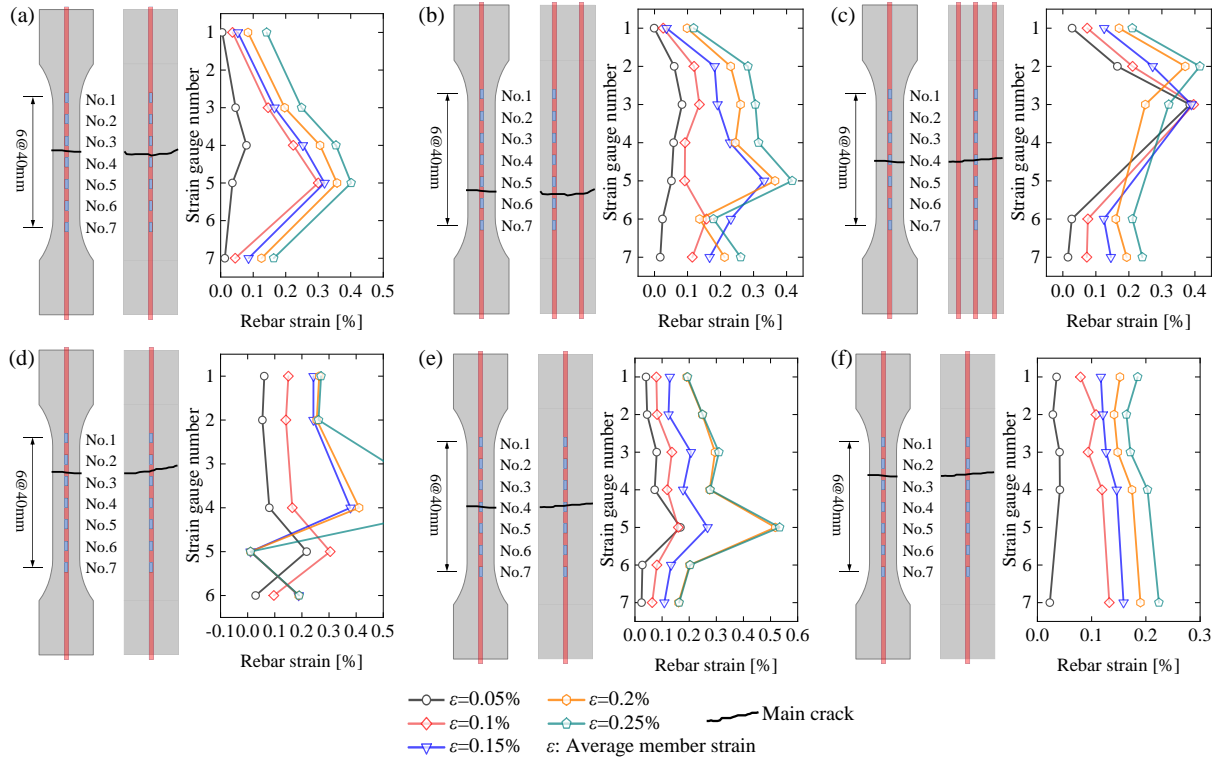
291 For rebar diameter, as the rebar diameter increased from 10 mm to 16 mm (the
 292 corresponding reinforcement ratio increased from 1.6% to 4.2%), the tensile bearing capacity
 293 also showed an increasing trend, and the increase of the post-peak residual bearing capacity
 294 was the difference between the yield-bearing capacity of the single bar ($\Delta f_{sy}\Delta A_s$). For concrete
 295 type, CA-UHPC exhibited obvious advantages over NC in synergistic tensile properties with
 296 rebar, which is not only reflected in the higher tensile strength and excellent post-cracking
 297 residual tensile strength CA-UHPC, but also in the excellent rebar/concrete interface bond
 298 properties.



299 **Fig. 8.** Analysis of investigated parameters: (a) rebar quantity; (b) rebar diameter; (c) concrete
 300 type.
 301

302 4.2 Rebar strain distribution

303 Fig.9 shows the rebar strain distribution of R-CA-UHPC members. In general, the strain
 304 distribution along rebar length was not uniform, which could be explained by the stress
 305 concentration of the rebar induced by the crack localization of CA-UHPC. The strain gauges
 306 located around the main crack presented relatively larger strain values, which were induced
 307 by the transfer of tensile force from CA-UHPC to rebar at the crack. Especially, strain
 308 concentration and early strain hardening of rebar developed once crack localization of CA-
 309 UHPC occurred, as the measured strain by rebar strain gauges located around the main crack
 310 was higher than the average member strain after member strain approached approximately the
 311 yielding strain ($\epsilon=0.2\%$).



312

313 **Fig. 9.** Rebar strain distribution of R-CA-UHPC members: (a) d_s10 ; (b) $2d_s10$; (c) $3d_s10$; (d)

314

d_s12 ; (e) d_s14 ; (f) d_s16 .

315 4.3 Distinctive loads and strains

316 Table 6 summarizes the values of the distinctive loads and strains of R-CA-UHPC
 317 members. The theoretical first cracking strain $\varepsilon_{cr,The}$ is the elastic limit tensile strain ε_{cte} based
 318 on the tensile constitutive model of CA-UHPC (see Fig.4), $\varepsilon_{cr,The} = \varepsilon_{cte} = f_{ct}/E_c$. Accordingly, the
 319 theoretical first cracking load $P_{cr,The}$ was obtained according to $P_{cr,The} = (E_c A_c + E_s A_s) \varepsilon_{cr,The}$,
 320 where A_c is the net cross-sectional area. The theoretical yielding load was calculated
 321 according to $P_{y,The} = f_{sy} A_s + \sigma_{ct} A_c$, where σ_{ct} is the tensile strength of CA-UHPC as average
 322 member strain reaching ε_y based on the tensile constitutive model of CA-UHPC, shown in
 323 Fig.4.

324

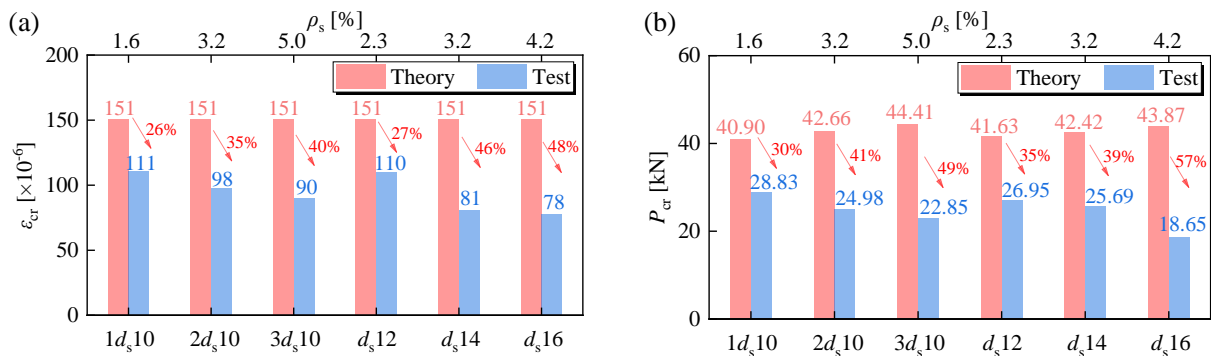
Table 6. Characteristic loads and strains of R-CA-UHPC members.

Rebar	ρ_s	No.	First cracking				Yielding			Peak	
			P_{cr} [kN]	$P_{cr,The}$ [kN]	ε_{cr} [$\times 10^{-6}$]	$\varepsilon_{cr,The}$ [$\times 10^{-6}$]	P_y [kN]	$P_{y,The}$ [kN]	ε_y [$\times 10^{-6}$]	P_m [kN]	ε_m [$\times 10^{-6}$]
d_s10	1.6%	SN-1	29.31	40.90	110	151	50.73	70.12	2438	67.10	5128
		SN-2	28.35		113		55.91			70.60	4105
		Mean	28.83		111		53.32			68.85	4616
		COV	2%	—	2%	—	7%	—	—	4%	16%
$2d_s10$	3.2%	SN-1	21.62	42.66	95	151	108.77	107.94	2438	116.25	2903
		SN-2	28.35		100		103.63			109.13	2730
		Mean	24.98		98		106.20			112.69	2816
		COV	19%	—	4%	—	3%	—	—	4%	4%
$3d_s10$	5.0%	SN-2	22.85	44.41	90	151	120.68	145.76	2438	159.80	3310
d_s12	2.3%	SN-1	28.90	41.63	120	151	68.68	84.92	2382	75.32	2990

		SN-2	24.99		100		66.57			77.89	3085
		Mean	26.95		110		67.62			76.60	3027
		COV	10%	—	13%	—	2%	—	—	2%	2%
d_s14	3.2%	SN-1	24.93	42.42	85	151	67.26	94.77	2104	85.30	3103
		SN-2	26.45		78		86.27			86.47	2140
		Mean	25.69		81		76.77			85.89	2621
		COV	4%		—		7%			—	18%
d_s16	4.2%	SN-1	18.88	43.87	73	151	84.79	114.21	1958	104.93	2818
		SN-2	18.42		84		96.69			99.21	3969
		Mean	18.65		78		90.74			102.07	3393
		COV	2%		—		11%			—	9%

325

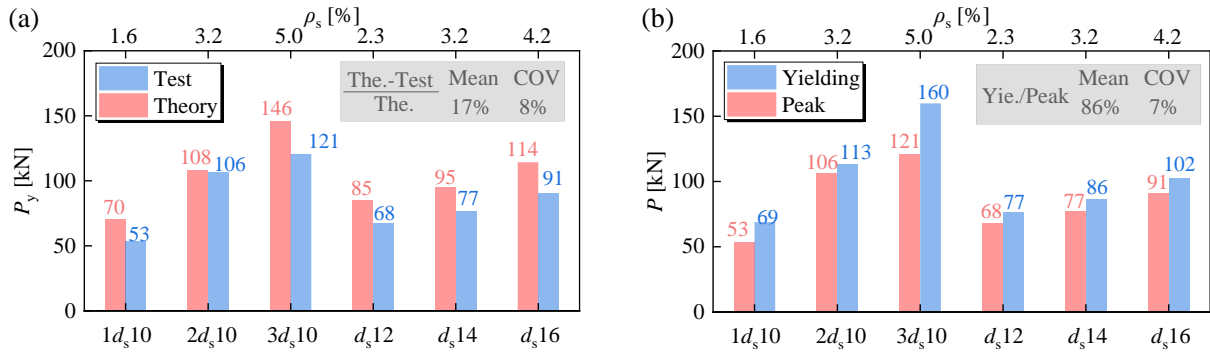
326 Fig.10 compares the theoretical first cracking loads and strains with the experimentally
327 measured ones. It was obvious that the test values were lower than the theoretical values,
328 neglecting the influence of matrix inhomogeneity of CA-UHPC and fiber distribution non-
329 uniformity caused by reinforcement. Moreover, the differences between the test and theory
330 increased significantly with the increase of the reinforcement ratio, the differences in first
331 cracking strains ranged from 26% to 48% as the reinforcement ratio changed from 1.6% to
332 5.0%, while the differences in the first cracking loads varied from 30% to 57%. The
333 pronounced decrease of cracking loads and strains may be induced by the emergence of pre-
334 tension in CA-UHPC at the curing stage, where the free shrinkage of CA-UHPC was
335 restrained by the rebar. The related mechanism and quantification of the effect will be
336 explained in detail in the next section.



337

338 **Fig. 10.** Comparison between theoretical and experimental first cracking values: (a) strains; (b)
339 loads.

340 Fig.11(a) shows the comparison between the theoretical and experimental yielding loads.
341 In general, the tested yielding load was 17% lower than the theoretical one. This also could be
342 interpreted by the restrained effect of rebar on the free shrinkage of CA-UHPC, which
343 generated pre-compressive stress in the rebar prior to the external load being applied. The
344 experimental yielding loads were obtained as the average member strain reaching ϵ_y . At the
345 moment, the rebar actually did not yield due to overcoming the pre-compression first.
346 Fig.11(b) compares the test yielding and peak loads. As shown, the yielding loads were
347 relatively close to the peak load, and the mean yielding load is 86% of the mean peak load.
348 The same experimental phenomenon can be found in existing studies [24,25,27] on the tensile
349 property of rebar-reinforced UHPC (without coarse aggregate) members.



350

351 **Fig. 11.** Comparison of distinctive load values: (a) theoretical and experimental yielding loads;

352

(b) experimental yielding and peak loads.

353

4.4 Crack distribution and ultimate failure modes

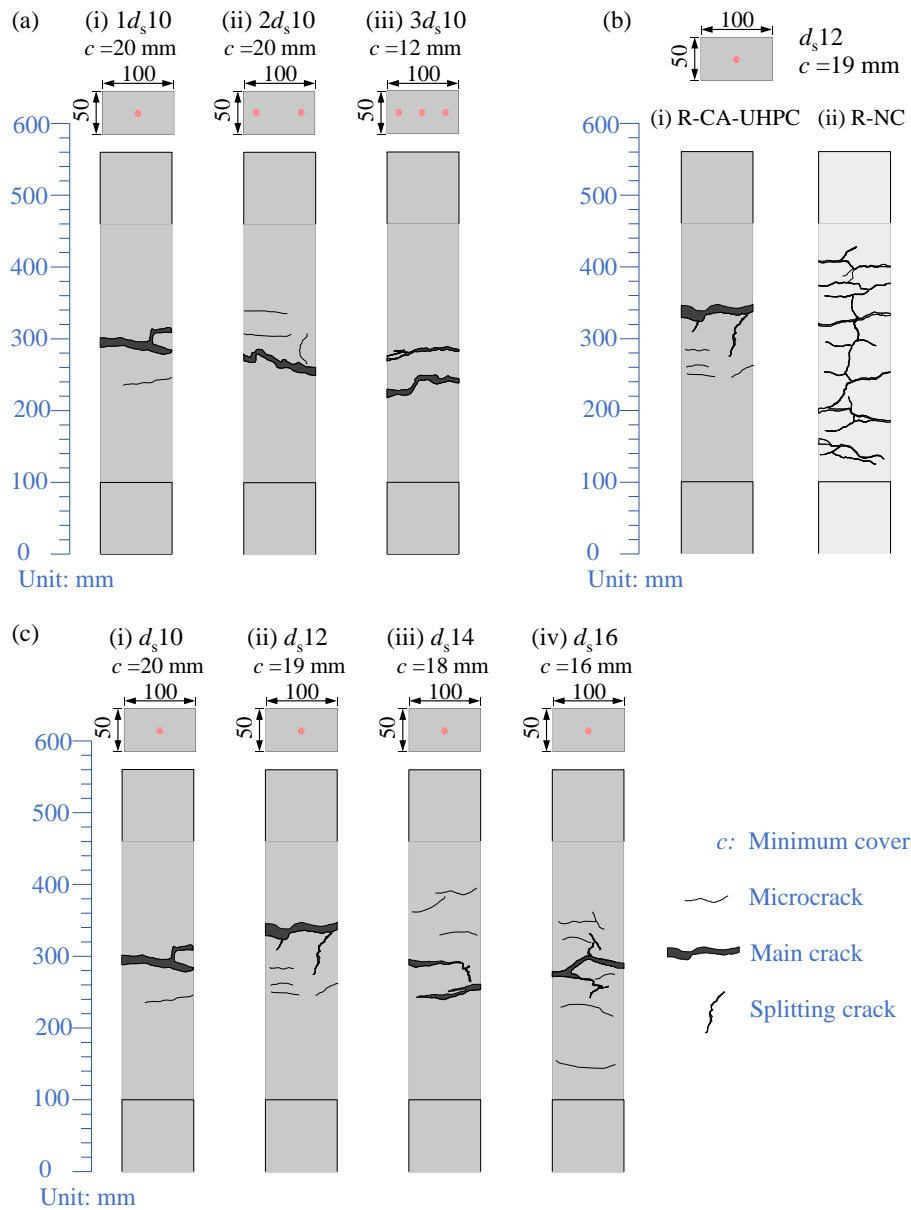
354

No visible cracks were observed for all the specimens prior to loading, indicating that the restrained tensile stress induced at the curing stage was lower than the tensile strength of concrete material. Fig.12 shows the typical crack distribution of the tested reinforced concrete members at the maximum elongation equal to half the steel fiber length. The R-NC members presented uniformly distributed and saturated transverse cracks which were connected by the splitting cracks. By comparison, crack localization was observed at the point around yielding in all the R-CA-UHPC specimens while no pronounced splitting crack was developed. This indicates that strain or crack localization is more prone to happen in R-CA-UHPC members, which is against previous knowledge that R-UHPC members has an advantage over R-NC members in achieving ductility because of the more excellent residual tensile capacity of UHPC by adding steel fibers.

365

Moreover, the crack localization of R-CA-UHPC has been slightly alleviated with the increase of reinforcement ratio for increasing rebar diameter as well as rebar quantity. According to Hung et al.'s research [22], the enhanced bond strength between rebar and UHPC due to the inclusion of steel fibers transformed the failure pattern of the R-UHPC from multiple localized cracks (no steel fibers) into a single localized crack (adding steel fibers), which will lead to the premature failure of R-UHPC reinforced with small steel rebars and subjected to monotonic loading.

371



372

373

374

Fig. 12. Crack distribution of reinforced concrete members with different parameters: (a) rebar quantity; (b) concrete types; (c) rebar diameter.

375

376

377

378

379

380

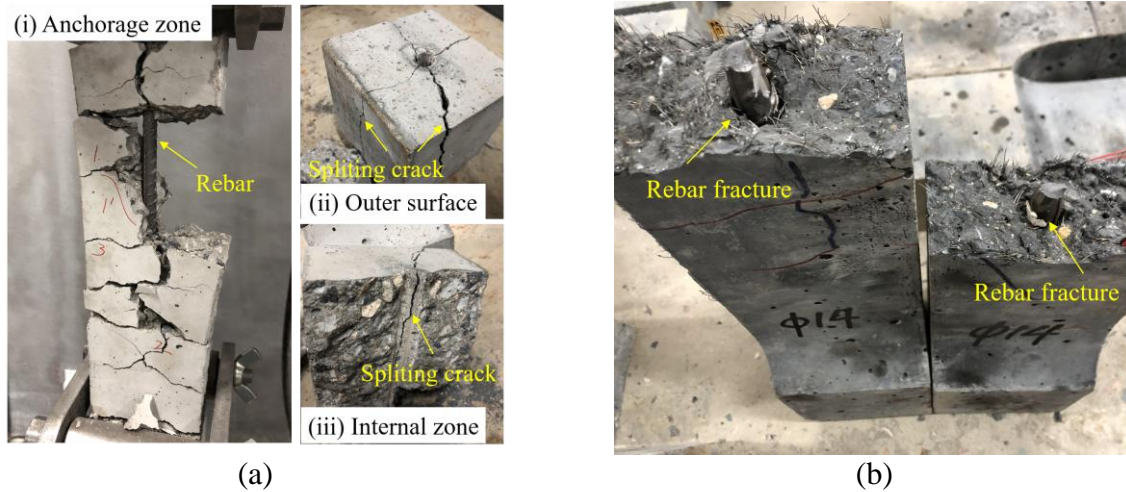
381

382

383

384

The typical ultimate failure modes of R-NC and R-CA-UHPC are compared in Fig.13. The concrete part of the R-NC member was divided into sub-components by transverse and longitudinal cracks due to the limited tensile strength of NC and bond strength between rebar and concrete. By comparison, the R-CA-UHPC member presented the fracture of the rebar at the main crack location. Qiu et al. [25] and Yu et al. [31] also demonstrated the same failure modes of R-UHPC members under axial tension. This was induced by the intensified strain concentration in the embedded rebar because of the crack localization of CA-UHPC. The significantly different failure modes of R-NC and R-CA-UHPC members demonstrate that CA-UHPC has substantially enhanced interface bond properties with rebar compared with NC.



385 **Fig. 13.** Ultimate failure modes: (a) R-NC; (b) R-CA-UHPC.

386 **5. Analysis of restrained shrinkage creep effect**

387 *5.1 Restrained shrinkage creep effect*

388 Compared with the unreinforced concrete members, the free shrinkage of concrete for
 389 reinforced concrete members is restrained due to the restrained effect of rebar on concrete.
 390 This induces an initial tensile stress (also named as the restrained tensile stress $\sigma_{ct,re}$) in the
 391 concrete, that leads to a reduction in external load needed to crack the member, as well as an
 392 initial compressive stress in the rebar before the load being applied [32]. Once concrete is
 393 subjected to tension, tensile creep strain is generated due to the inherent creep behavior of
 394 concrete, which in turn reduces the shrinkage strain and restrained tensile stress of concrete.
 395 This mechanism is called stress relaxation [33]. The restrained shrinkage couples with the
 396 tensile creep, so the restrained effect on free shrinkage and the derived tensile creep effect are
 397 identified as the restrained shrinkage creep effect.

398 Fig.14 plots the restrained shrinkage creep effect, where ϵ_{cs} is the free shrinkage strain of
 399 concrete, $\epsilon_{cs,re}$ is the developed shrinkage of concrete under the constraint of steel bars, i.e.,
 400 the restrained shrinkage strain, $\epsilon_{ct,re}$ is the restrained tensile strain of concrete due to the
 401 restrained shrinkage creep effect, ϵ_{ccr} is the tensile creep strain of concrete.

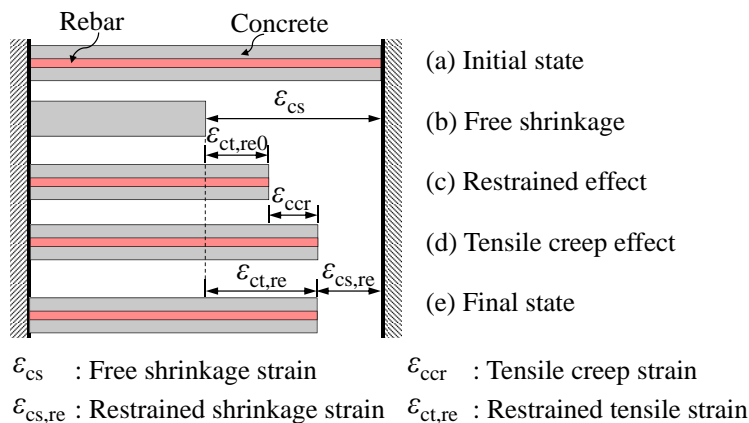


Fig. 14. Restrained shrinkage creep effect for reinforced concrete members [36].

404 Given the final state of deformation in Fig.14, assuming that the restrained tensile stress
 405 developed in the concrete is $\sigma_{ct,re}$ and the developed restrained shrinkage strain of concrete is
 406 $\varepsilon_{cs,re}$, then the compressive strain of the rebar equals $\varepsilon_{cs,re}$ based on the assumption of
 407 deformation coordination. According to the equilibrium of internal forces, Eq.(1) can be
 408 obtained, and then the restrained shrinkage strain $\varepsilon_{cs,re}$ is accordingly expressed in Eq.(2):

$$A_c \sigma_{ct,re} = A_s E_s \varepsilon_{cs,re} \quad (1)$$

$$\varepsilon_{cs,re} = \frac{A_c \sigma_{ct,re}}{A_s E_s} = \frac{\sigma_{ct,re}}{\rho_s E_s} \quad (2)$$

411
 412 where ρ_s is reinforcement ratio, $\rho_s = A_s/A_c$, A_s is the cross-sectional area of rebar, A_c is the net
 413 cross-sectional area of concrete.

414 The first cracking strength f_{cr} of R-CA-UHPC can be obtained according to Eq.(3) based
 415 on the test first cracking load P_{cr} listed in Table 6.

$$P_{cr} = (1 + \alpha_E \rho_s) A_c f_{cr} \quad (3)$$

417 where α_E is elastic modulus ratio of rebar to CA-UHPC, $\alpha_E = E_s/E_c$; $\alpha_E \rho_s$ is axial stiffness ratio
 418 of rebar to CA-UHPC.

419 The induced restrained tensile stress $\sigma_{ct,re}$ in CA-UHPC for R-CA-UHPC members at the
 420 end of the curing stage can be determined as the difference between the tensile strength of
 421 CA-UHPC f_{ct} and the first cracking strength f_{cr} of R-CA-UHPC members, as expressed in
 422 Eq.(4). The obtained $\sigma_{ct,re}$ in Eq.(4) and $\varepsilon_{cs,re}$ in Eq.(2) can be considered as indirect test values.

$$\sigma_{ct,re} = f_{ct} - f_{cr} \quad (4)$$

424 Table 7 lists the comparison between test and theory first cracking strengths and strains
 425 for R-CA-UHPC members. The restrained tensile stress $\sigma_{ct,re}$ in CA-UHPC increases with the
 426 increasing of axial stiffness ratio $\alpha_E \rho_s$, while the restrained shrinkage strain $\varepsilon_{cs,re}$ exhibits an
 427 opposite trend.

428 **Table 7.** Comparison between tested and theoretical first cracking strengths and strains.

Rebar	$\alpha_E \rho_s$	Test		Theory		Restrained effect	
		f_{cr} [MPa]	ε_{cr} [$\times 10^{-6}$]	f_{ct} [MPa]	ε_{cte} [$\times 10^{-6}$]	$\sigma_{ct,re}$ [MPa]	$\varepsilon_{cs,re}$ [$\times 10^{-6}$]
$d_s 10$	0.061	5.52	111	7.83	151	2.31	723
$2d_s 10$	0.125	4.59	98			3.24	500
$3d_s 10$	0.190	4.03	90			3.80	384
$d_s 12$	0.088	5.08	110			2.75	602
$d_s 14$	0.118	4.74	81			3.09	504
$d_s 16$	0.167	3.33	73			4.50	517

429 To further quantify the impact of the restrained shrinkage creep effect during the
 430 standard curing stage on the internal force redistribution and the first cracking of the R-CA-
 431 UHPC members, the Dischinger-differential-equation-based [37] theoretical analysis was
 432 conducted from the perspective of deformation coordination between rebar and CA-UHPC.
 433 The first step of theoretical analysis was the quantification of three key parameters of CA-

434 UHPC, i.e., elastic modulus, free shrinkage, and tensile creep, which are time-dependent at
 435 early age. It should be noted that owing to the relatively low water-binder ratio and the high
 436 volume use of cementitious material, the UHPC material has extremely high autogenous
 437 shrinkage but insignificant drying shrinkage [36]. Therefore, the determination of the
 438 autogenous shrinkage of CA-UHPC was performed in the following section.

439 *5.2 Modelling of age-dependent parameters*

440 *5.2.1 Elastic modulus*

441 This study involved the experimental measurement of the elastic modulus (100 mm ×
 442 100 mm × 300 mm prisms) for CA-UHPC at the age of 1d, 2d, 3d, 4d, 5d, 7d, 10d, 14d, 21d,
 443 and 28d under standard curing condition as stated above. The elastic modulus test results of
 444 UHPC under the same curing condition conducted by Graybeal [38] have been also collected
 445 and listed in Table 8. Based on all the data, a normalized time-dependent evolution function of
 446 elastic modulus for UHPC was developed, given in Eq.(5) and plotted in Fig.15.

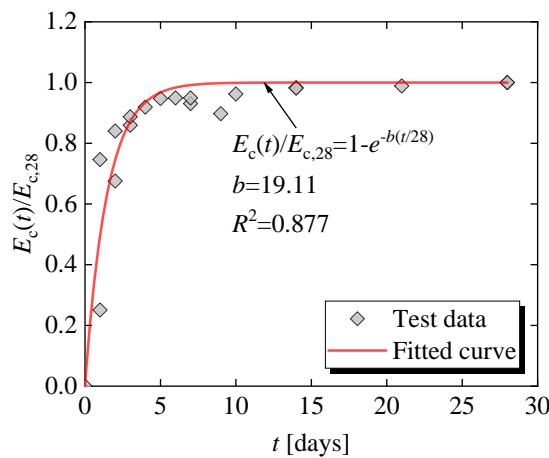
447
$$\frac{E_c(t)}{E_{c,28}} = 1 - e^{-19.11(\frac{t}{28})} \quad (5)$$

448 where $E_{c,28}$ is the elastic modulus of UHPC at 28d, t is age in days.

449 **Table 8.** Elastic modulus of UHPC at different ages.

Reference	t [days]	$E_c(t)$ [MPa]	$E_c(t)/E_{c,28}$	t [days]	$E_c(t)$ [MPa]	$E_c(t)/E_{c,28}$
This study	1	39700	0.746	7	50500	0.949
	2	44700	0.840	10	51200	0.962
	3	47200	0.887	14	52600	0.989
	4	48900	0.919	21	52200	0.981
	5	50400	0.947	28	53200	1
Graybeal [38]	1	10500	0.251	7	39000	0.931
	2	28300	0.675	9	37600	0.897
	3	36000	0.859	28	41900	1

450



451

452

Fig. 15. Evolution of elastic modulus at early age.

453 5.2.2 Autogenous shrinkage

454 Yoo et al. [39]proposed a time-dependent model for autogenous shrinkage of UHPC, as
 455 given in Eq.(6)~ Eq.(8).

456
$$\varepsilon_{as}(t) = \gamma \varepsilon_{as\infty} \beta(t) \quad (6)$$

457
$$\varepsilon_{as\infty} = 2300 e^{\left[\frac{-7.2w}{B} \right]} \quad (7)$$

458
$$\beta(t) = 1 - e^{(-0.65\sqrt{t})} \quad (8)$$

459 where t is age in days; $\varepsilon_{as\infty}$ is the ultimate autogenous shrinkage; $\beta(t)$ is the development
 460 function of autogenous shrinkage; w/B is the water-to-binder ratio; γ is a coefficient to
 461 describe the effect of shrinkage-reducing admixture (SRA), γ is 1 when no adding SRA, while
 462 is 0.85 when including 1% SRA.

463 The prediction model of autogenous shrinkage proposed by Yoo et al is only suitable for
 464 conventional UHPC without coarse aggregate. Existing studies revealed that the addition of
 465 coarse aggregate contributed to reducing the autogenous shrinkage of the UHPC matrix.
 466 Therefore, it is essential to improve the model proposed by Yoo et al and to extend the
 467 applicability to CA-UHPC. Li et al. [12]investigated the influence of the dosage of coarse
 468 aggregate on autogenous shrinkage of UHPC within 90d, and the test results are listed in
 469 Table 9. However, Li et al. [12]didn't develop a model that could quantify the effect of dosage
 470 of coarse aggregate on autogenous shrinkage. Based on the test data in Table 9, the mass ratio
 471 of coarse aggregate to total aggregate η (including coarse and fine aggregates) and the impact
 472 factor of coarse aggregate on autogenous shrinkage α were proposed in this study, as given in
 473 Eq.(9) and Eq.(10):

474
$$\eta = \frac{m_{CA}}{m_{CA} + m_{FA}} \quad (9)$$

475 where m_{CA} is the mass of coarse aggregate, m_{FA} is the mass of fine aggregate.

476
$$\alpha = \frac{\varepsilon_{as,CA-UHPC}}{\varepsilon_{as,UHPC}} \quad (10)$$

477 where $\varepsilon_{as,CA-UHPC}$ is the autogenous shrinkage of CA-UHPC, $\varepsilon_{as,UHPC}$ is the autogenous
 478 shrinkage of UHPC without coarse aggregate.

479 **Table 9.** Effect of coarse aggregate on autogenous shrinkage of UHPC within 90d [12].

η	$\varepsilon_{as,CA-UHPC}$ [$\times 10^{-6}$]	$\varepsilon_{as,UHPC}$ [$\times 10^{-6}$]	α
0	615.9	615.9	1
0.125	556.9	615.9	0.904
0.225	543.5	615.9	0.882
0.325	516.7	615.9	0.839
0.425	496.7	615.9	0.806

480 The relation between mass ratio η and impact factor α was fitted as plotted in Fig.16(a)
 481 and given in Eq.(11). Therefore, the modified model which was suitable for UHPC with or
 482 without coarse aggregate for describing the autogenous shrinkage development at early age
 483 was established, as expressed in Eq.(12):

484

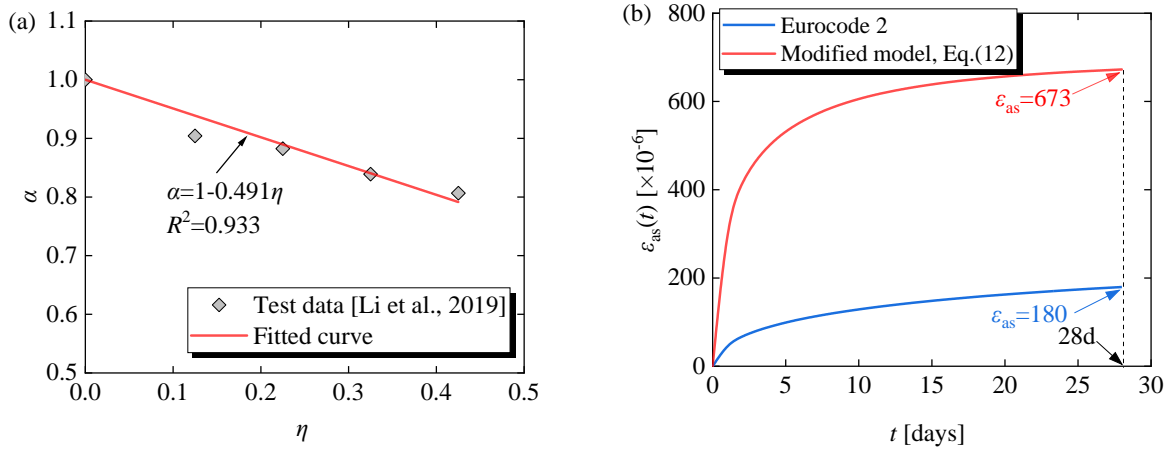
$$\alpha = 1 - 0.491\eta \quad (11)$$

485

$$\varepsilon_{as}(t) = \gamma\alpha\varepsilon_{as\infty}\beta(t) \quad (12)$$

486 where α is the impact factor of coarse aggregate on autogenous shrinkage, other parameters
487 are described shown in Eq.(6).

488 The w/B and mass ratio η of CA-UHPC used in this study were 0.133 and 0.433,
489 respectively. Accordingly, the autogenous shrinkage of $673 \mu\varepsilon$ for CA-UHPC at 28d under the
490 standard curing was obtained according to Eq.(11) and Eq.(12) and is going to be assumed as
491 a reference for further elaborations in this study. According to the basic material parameters of
492 CA-UHPC used in this study, the modified autogenous shrinkage model in Eq.(12) was
493 compared with the autogenous shrinkage model in Eurocode 2 [40], as shown in Fig.(16).
494 Eurocode 2 significantly underestimates the autogenous shrinkage of CA-UHPC.



495 **Fig. 16.** Modified autogenous shrinkage model of UHPC: (a) relation between mass ratio
496 η and impact factor α ; (b) comparison with Eurocode 2.

497 5.2.3 Creep

498 The creep here refers to the tensile creep deformation, which occurs in CA-UHPC once
499 the interface bond between rebar and CA-UHPC comes to an effect and restrains the free
500 shrinkage. It is difficult to accurately determine the starting time of the tensile creep. Given
501 that there is limited research on the creep properties of UHPC currently, it is generally
502 believed that the tensile creep coefficient is equivalent to the compressive creep coefficient
503 for concrete [33]. The compressive creep coefficient of UHPC has been hereafter used to
504 consider the impact of tensile creep.

505 The Swiss design code SIA 2052 [41] provides the evolution function of the compressive
506 creep coefficient for UHPC as given in Eq.(13).

$$507 \quad \varphi(t, t_0) = \varphi_{\infty}(t, t_0) \cdot \frac{(t - t_0)^a}{(t - t_0)^a + b} \quad (13)$$

508 where $\varphi(t, t_0)$ is the creep coefficient, $\varphi_{\infty}(t, t_0)$ is the final creep coefficient, t is age, t_0 is the age
509 at first loading, a and b are coefficients as listed in Table 10.

510

511

512

Table 10. Final creep coefficient and coefficients a and b [41].

t_0 [days]	Curing	$\varphi_{\infty}(t, t_0)$	a	b
4	20°C	1.2	0.6	3.2
7	20°C	1.0	0.6	4.5
28	20°C	0.9	0.6	10
—	Thermal treatment - 2 days at 90 °C and steamed	0.3	0.6	10

513 The initial setting time of the CA-UHPC used is approximately 6~9 hours, and the final
514 setting time is 8~11 hours. Therefore, the initial loading age of the tensile creep t_0 is less than
515 4d. Nevertheless, the Swiss design code is only suitable for t_0 equal to or larger than 4d. To
516 derive the creep coefficient development function for t_0 earlier than 4d, the basic creep model
517 proposed by Dischinger [37] has been used, as given in Eq.(14).

$$518 \quad \varphi(t, 0) = \varphi_{k0} \left(1 - e^{-\beta t}\right) \quad (14)$$

519 where φ_{k0} is the ultimate value of the creep coefficient, β is the coefficient of creep growth
520 rate.

521 The creep coefficient from t_0 to t can be derived when using Dischinger's basic creep
522 model for aging theory [37], as expressed below:

$$523 \quad \begin{aligned} \varphi(t, t_0) &= \varphi(t, 0) - \varphi(t_0, 0) \\ &= \varphi_{k0} e^{-\beta t_0} \left[1 - e^{-\beta(t-t_0)}\right] \\ &= \varphi_{\infty}(t, t_0) \left[1 - e^{-\beta(t-t_0)}\right] \end{aligned} \quad (15)$$

524 Consequently, the final creep coefficient $\varphi_{\infty}(t, t_0)$ from t_0 to t is given by:

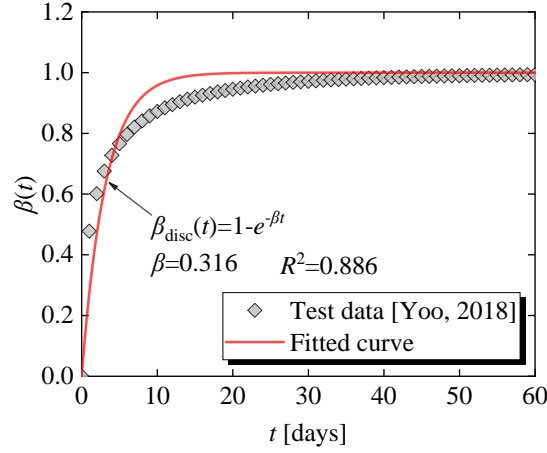
$$525 \quad \varphi_{\infty}(t, t_0) = \varphi_{k0} e^{-\beta t_0} \quad (16)$$

526 In the following section, the restrained tensile stress of CA-UHPC will be derived
527 according to the Dischinger differential equation. The key to solving this differential equation
528 is to assume that the development law of shrinkage is similar to that of creep. To obtain the
529 coefficient of creep growth rate β , the time-dependent development model of autogenous
530 shrinkage for UHPC proposed by Yoo et al.[39] was re-fitted according to the form of creep
531 coefficient $\varphi(t, t_0)$ in Eq.(15), as given in Eq.(17):

$$532 \quad \begin{aligned} \varepsilon_{as}(t) &= \varepsilon_{as\infty} \beta_{disc}(t) \\ &= \varepsilon_{as\infty} \left[1 - e^{-\beta(t-t_0)}\right] \end{aligned} \quad (17)$$

533 where $\beta_{disc}(t)$ is the development function of autogenous shrinkage, in which $t_0=0$.

534 The fitting result is plotted in Fig.17. As shown, the fitted coefficient of creep growth
535 rate β was 0.316.



536

537

538

Fig. 17. Dischinger-form based time-dependent development function of autogenous shrinkage for UHPC.

539

540

541

542

Assuming $\beta = 0.316$ and $\varphi_{\infty}(t, t_0) = 1.2$ corresponding to $t_0 = 4d$ into Eq.(16), $\Phi_{k0} = 4.25$ was obtained. Therefore, the development function of the creep coefficient corresponding to any first loading age t_0 can be given below.

$$\varphi(t, t_0) = 4.25e^{-0.316t_0} \left[1 - e^{-0.316(t-t_0)} \right] \quad (18)$$

543

5.3 Dischinger-differential-equation-based theoretical analysis

544

545

5.3.1 Theoretical derivation

546

547

548

549

For reinforced concrete members, the deformation between rebar and concrete is assumed equal through interfacial bonding force, and the strain increment of the two components at the bonding point is consistent [37]. According to deformation coordination, the rebar and concrete are first regarded as free bodies that are separated from each other, and only constrained by interaction forces along the axis of the rebar.

550

551

552

553

554

Let $F_s(t, t_0)$ represent the interaction force between rebar and concrete during the period from the initial interaction age t_0 to t , ε_{c1} and ε_{s1} denote the elastic strain of the concrete-free body generated at the location of the rebar, and the elastic strain generated at the rebar-free body when $F_s(t, t_0) = 1$, respectively. As a simplification, the elastic modulus of concrete E_c is assumed to be constant. Therefore, ε_{c1} and ε_{s1} can be expressed respectively as:

555

$$\varepsilon_{c1} = \frac{1}{E_c A_c} \quad (19)$$

556

$$\varepsilon_{s1} = \frac{1}{E_s A_s} \quad (20)$$

557 Make:

558

$$\varepsilon_{11} = \varepsilon_{c1} + \varepsilon_{s1} \quad (21)$$

559

$$\alpha = \frac{\varepsilon_{c1}}{\varepsilon_{11}} \quad (22)$$

560

According to the differential equation solved by Dischinger [37], the compatibility

561 condition for strain increment between rebar and concrete in time interval dt is:

$$562 \quad dF_s(t, t_0)\varepsilon_{11} + F_s(t, t_0)\varepsilon_{c1}d\varphi(t, t_0) - d\varepsilon_{cs}(t, t_0) = 0 \quad (23)$$

563 where $dF_s(t, t_0)\varepsilon_{11}$ is the increment of elastic strain generated by the increment of interactive
564 force, $F_s(t, t_0)\varepsilon_{c1}d\varphi(t, t_0)$ is the strain increment caused by tensile creep under interactive force,
565 $d\varepsilon_{cs}(t, t_0)$ is the strain increment caused by shrinkage.

566 It is assumed that the development law of shrinkage is the same as that of creep, that is,
567 the development functions of shrinkage and creep adopt Eq.(17) and Eq.(18), respectively,
568 then:

$$569 \quad d\varepsilon_{cs}(t, t_0) = \frac{\varepsilon_{cs\infty}}{\varphi_\infty} d\varphi(t, t_0) \quad (24)$$

570 Substituting Eq.(22) and Eq.(24) into Eq.(23) yields:

$$571 \quad dF_s(t, t_0)\varepsilon_{11} + \alpha\varepsilon_{11}F_s(t, t_0)d\varphi(t, t_0) - \frac{\varepsilon_{cs\infty}}{\varphi_\infty} d\varphi(t, t_0) = 0 \quad (25)$$

572 The following differential equation is obtained when Eq.(25) is divided by ε_{11} :

$$573 \quad dF_s(t, t_0) + \alpha d\varphi(t, t_0)F_s(t, t_0) = \frac{\varepsilon_{cs\infty}}{\varepsilon_{11}\varphi_\infty} d\varphi(t, t_0) \quad (26)$$

574 Solving this differential equation yields:

$$575 \quad F_s(t, t_0) = \frac{\varepsilon_{cs\infty}}{\alpha\varepsilon_{11}\varphi_\infty} + Ce^{-\alpha\varphi(t, t_0)} \quad (27)$$

576 According to the boundary conditions, $\varphi(t, t_0)=0$, $F_s(t, t_0)=0$ when $t=t_0$, the integral
577 constant C can be obtained as following:

$$578 \quad C = -\frac{\varepsilon_{cs\infty}}{\alpha\varepsilon_{11}\varphi_\infty} \quad (28)$$

579 Substituting Eq.(28) into Eq.(27) gives:

$$580 \quad F_s(t, t_0) = \frac{\varepsilon_{cs\infty}}{\alpha\varepsilon_{11}\varphi_\infty} \left[1 - e^{-\alpha\varphi(t, t_0)} \right] \quad (29)$$

581 Substituting Eq.(22) into Eq.(29) gives:

$$582 \quad F_s(t, t_0) = \frac{\varepsilon_{cs\infty}}{\varepsilon_{c1}\varphi_\infty} \left[1 - e^{-\alpha\varphi(t, t_0)} \right] \quad (30)$$

583 Substituting Eq.(19) into Eq.(30) gives:

$$584 \quad F_s(t, t_0) = \frac{\varepsilon_{cs\infty}}{\varphi_\infty} E_c A_c \left[1 - e^{-\alpha\varphi(t, t_0)} \right] \quad (31)$$

585 Therefore, the restrained tensile stress $\sigma_{ct, re}(t, t_0)$ due to the restrained shrinkage and
586 inclusive of creep/relaxation effect from t_0 to t is expressed as:

$$587 \quad \sigma_{ct, re}(t, t_0) = \frac{F_s(t, t_0)}{A_c} = \frac{\varepsilon_{cs\infty}}{\varphi_\infty} E_c \left[1 - e^{-\alpha\varphi(t, t_0)} \right] \quad (32)$$

588 The corresponding restrained shrinkage strain $\varepsilon_{cs, re}(t, t_0)$ is obtained by substituting
589 Eq.(32) into Eq.(2):

590
$$\varepsilon_{cs,re}(t, t_0) = \frac{F_s(t, t_0)}{A_c} = \frac{\varepsilon_{cs\infty}}{\varphi_\infty} \frac{E_c}{\rho_s E_s} \left[1 - e^{-\alpha\varphi(t, t_0)} \right] \quad (33)$$

591 It should be noted that the restrained tensile stress $\sigma_{ct,re}(28, t_0)$ and the restrained
 592 shrinkage strain $\varepsilon_{cs,re}(28, t_0)$ for R-CA-UHPC members under standard curing for 28d are
 593 simplified as $\sigma_{ct,re,28}$ and $\varepsilon_{cs,re,28}$, respectively. Besides, the two results obtained based on
 594 Dischinger's differential equation are marked as analytical values.

595 *5.3.2 Quantification of uncertain parameters*

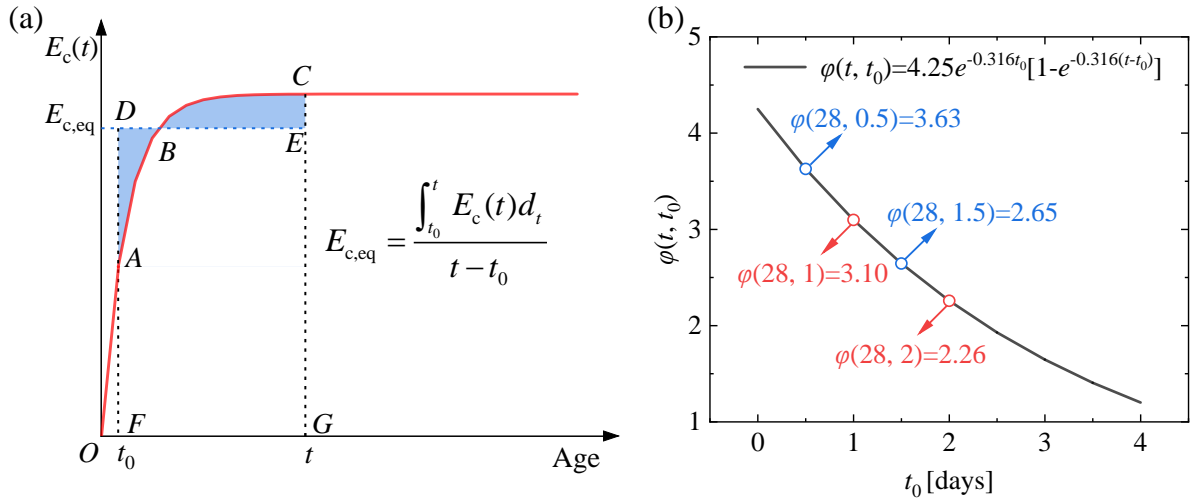
596 The quantification of E_c and t_0 needs to be discussed to obtain $\sigma_{ct,re,28}$ and $\varepsilon_{cs,re,28}$
 597 according to Eq.(32) and Eq.(33) accurately. On the one hand, the elastic modulus of CA-
 598 UHPC is not constant, and is developed with time along the curing stage. On the other hand,
 599 the initial time t_0 (also named as the initial loading age) for the interaction between rebar and
 600 CA-UHPC, which also governs the magnitude of the tensile creep coefficient $\varphi(t, t_0)$, is
 601 difficult to determine at the curing stage.

602 For the quantification of E_c , the concept of equivalent average elastic modulus $E_{c,eq}$ at the
 603 early age from t_0 to t was proposed, as shown in Fig.18(a) and Eq.(34), the changing elastic
 604 modulus $E_c(t)$ was equivalent to a constant elastic modulus $E_{c,eq}$ by making area S_{FABCG} equal
 605 to S_{FDEG} . Based on this method, the initial interactive time t_0 also determined the magnitude of
 606 $E_{c,eq}$.

607
$$E_{c,eq} = \frac{\int_{t_0}^t E_c(t) dt}{t - t_0} \quad (34)$$

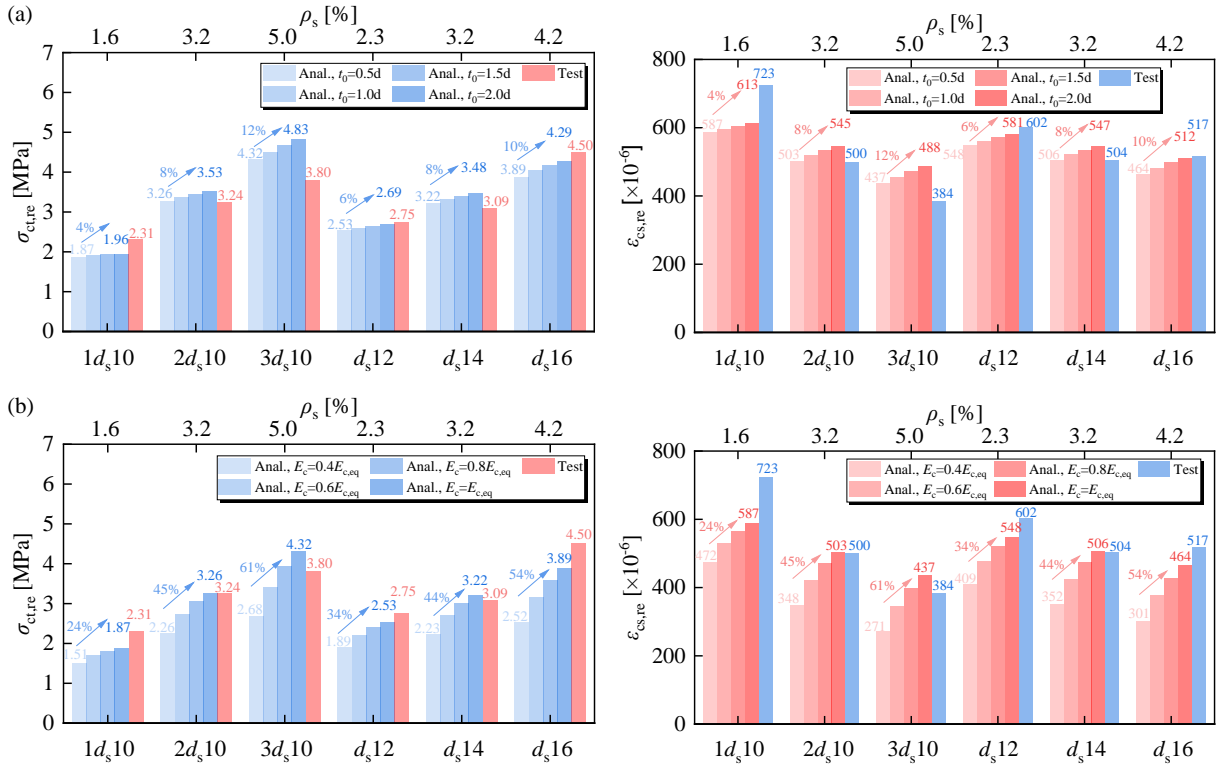
608 The initial setting time of CA-UHPC is approximately 6~9 hours, and the final setting
 609 time is approximately 8~11 hours. Therefore, it can be preliminarily considered that the initial
 610 interactive time t_0 was 0.5d.

611 The analysis of the influence of E_c and t_0 on $\sigma_{ct,re,28}$ and $\varepsilon_{cs,re,28}$ will be conducted based
 612 on two cases. Case I: when $E_c = E_{c,eq}$, t_0 was taken as 0.5d, 1.0d, 1.5d, and 2.0d, respectively
 613 (the corresponding influence of t_0 on tensile creep coefficient is shown in Fig.18(b)). Case
 614 II: when $t_0 = 0.5d$, E_c was taken as $0.4E_{c,eq}$, $0.6E_{c,eq}$, $0.8E_{c,eq}$, and $E_{c,eq}$, respectively. The
 615 influence of E_c and t_0 on the analytical values of $\sigma_{ct,re,28}$ and $\varepsilon_{cs,re,28}$ under these two cases, and
 616 the comparison between the analytical and test values are shown in Fig.19.



617
618
619

Fig. 18. Quantification of uncertain parameters: (a) equivalent average elastic modulus; (b) influence of initial loading age on tensile creep coefficient.

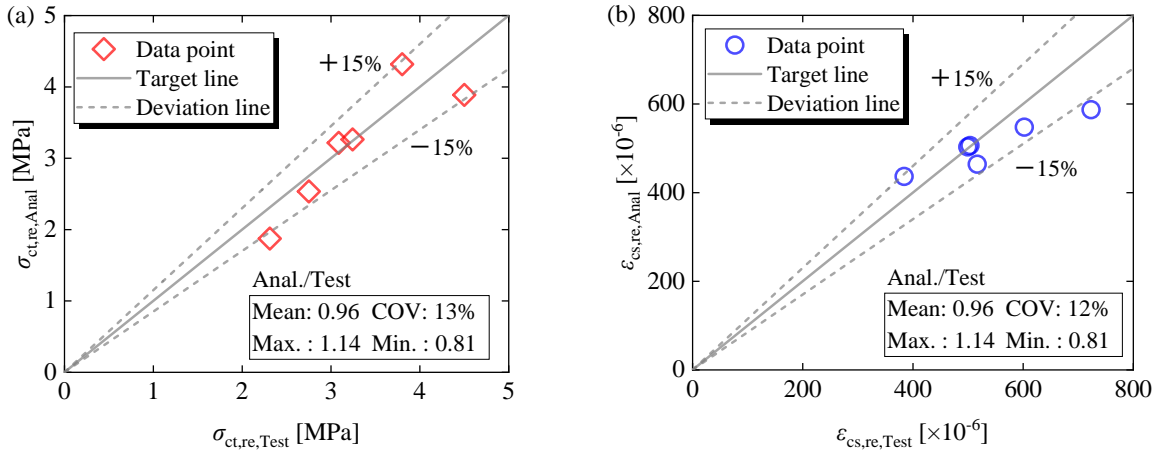


620
621
622

Fig. 19. Influence of elastic modulus and initial loading age on restrained tensile stress and restrained shrinkage strain: (a) $E_c = E_{c,eq}$, varying t_0 ; (b) $t_0 = 0.5d$, varying E_c .

623
624
625
626
627
628
629
630

As shown in Fig.19(a), when $E_c = E_{c,eq}$, the analytically calculated values of $\sigma_{ct,re,28}$ and $\epsilon_{cs,re,28}$ increased with the initial interaction time t_0 , with an amplification from 4% to 12%. As shown in Fig.19(b), when $t_0 = 0.5d$, the analytically calculated values of $\sigma_{ct,re,28}$ and $\epsilon_{cs,re,28}$ increased with E_c , with an amplification from 24% to 61%. It can be concluded that the value of E_c has a more significant impact on the calculated values of $\sigma_{ct,re,28}$ and $\epsilon_{cs,re,28}$ compared to that of t_0 . Taking into account the difference between the analytical and test values comprehensively, the analytical values of $\sigma_{ct,re,28}$ and $\epsilon_{cs,re,28}$ corresponding to $E_c = E_{c,eq}$ and $t_0 = 0.5d$ were chosen to further compare with the test values, as shown in Fig.20.



631 **Fig. 20.** Comparison between analytical and test values of CA-UHPC: (a) restrained
 632 tensile stress; (b) restrained shrinkage strain.

633 As plotted, the mean value and coefficient of variation of the ratio of analytical value to
 634 test value for the restrained tensile stress were 0.96 and 13%, and the corresponding items for
 635 the restrained shrinkage strain were 0.96 and 12%. It demonstrates the applicability and the
 636 high accuracy of the Dischinger-differential-equation-based analytical solution and the related
 637 quantification of time-dependent parameters, including elastic modulus $E_c(t)$, autogenous
 638 shrinkage $\varepsilon_{as}(t)$, tensile creep coefficient $\varphi(t, t_0)$, equivalent average elastic modulus $E_{c, eq}$ and
 639 the initial interactive time t_0 , and could be used to predict the restrained tensile stress $\sigma_{ct, re, 28}$
 640 and the restrained shrinkage strain $\varepsilon_{cs, re, 28}$ of R-CA-UHPC members under the standard curing
 641 condition.

642 5.3.3 Simplified prediction model

643 The analytical values of the restrained tensile stress and the restrained shrinkage strain at
 644 different ages when $t_0=0.5d$ and $E_c=E_{c, eq}$, are shown in Tables 11 and 12, respectively. The
 645 fitted development functions of the restrained tensile stress and the restrained shrinkage strain
 646 at early age are shown in Fig.21, and given in Eq.(35) and Eq.(36), respectively. It is obvious
 647 that the two items have the same development function. According to the development
 648 function of the restrained tensile stress, the cracking risk of R-CA-UHPC members at early
 649 age can be evaluated once mastering the development function of the tensile strength for CA-
 650 UHPC.

651 **Table 11.** Analytical values of $\sigma_{ct, re}(t)$ at different ages when $t_0=0.5d$ and $E_c=E_{c, eq}$.

Rebar	t	$\sigma_{ct, re}(t)$	$\sigma_{ct, re}(t)/\sigma_{ct, re, 28}$	Rebar	t	$\sigma_{ct, re}(t)$	$\sigma_{ct, re}(t)/\sigma_{ct, re, 28}$
	[days]	[MPa]	—		[days]	[MPa]	—
d_s10	1	0.27	0.14	$2d_s10$	1	0.47	0.14
	2	0.70	0.38		2	1.23	0.38
	3	1.02	0.54		3	1.78	0.54
	4	1.25	0.67		4	2.17	0.66
	5	1.41	0.75		5	2.45	0.75
	7	1.62	0.87		7	2.81	0.86
	14	1.84	0.98		14	3.19	0.98
	21	1.87	1.00		21	3.25	1.00

	28	1.87	1.00		28	3.26	1.00
$3d_s10$	1	0.62	0.14	d_s12	1	0.37	0.14
	2	1.63	0.38		2	0.95	0.38
	3	2.35	0.54		3	1.38	0.54
	4	2.87	0.66		4	1.69	0.67
	5	3.24	0.75		5	1.91	0.75
	7	3.70	0.86		7	2.19	0.86
	14	4.20	0.97		14	2.48	0.98
	21	4.29	0.99		21	2.52	1.00
	28	4.32	1.00	28	2.53	1.00	
d_s14	1	0.46	0.14	d_s16	1	0.56	0.14
	2	1.21	0.38		2	1.47	0.38
	3	1.75	0.54		3	2.12	0.54
	4	2.14	0.66		4	2.58	0.66
	5	2.42	0.75		5	2.92	0.75
	7	2.77	0.86		7	3.34	0.86
	14	3.14	0.98		14	3.79	0.98
	21	3.20	1.00		21	3.87	0.99
	28	3.22	1.00	28	3.89	1.00	

652

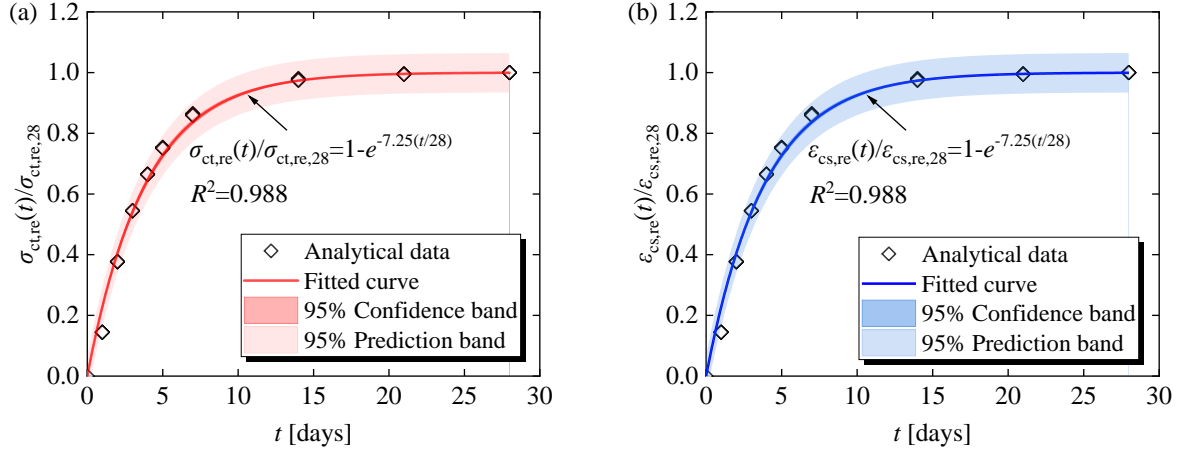
653

Table 12. Analytical values of $\varepsilon_{cs, re}(t)$ at different ages when $t_0=0.5d$ and $E_c=E_{c, eq}$.

Rebar	t	$\varepsilon_{cs, re}(t)$	$\varepsilon_{cs, re}(t)/\varepsilon_{cs, re, 28}$	Rebar	t	$\varepsilon_{cs, re}(t)$	$\varepsilon_{cs, re}(t)/\varepsilon_{cs, re, 28}$
	[days]	[$\times 10^{-6}$]	—		[days]	[$\times 10^{-6}$]	—
d_s10	1	85	0.14	$2d_s10$	1	73	0.14
	2	221	0.38		2	189	0.38
	3	320	0.54		3	274	0.54
	4	391	0.67		4	334	0.66
	5	443	0.75		5	378	0.75
	7	508	0.87		7	433	0.86
	14	576	0.98		14	492	0.98
	21	585	1.00		21	501	1.00
	28	587	1.00		28	503	1.00
$3d_s10$	1	63	0.14	d_s12	1	79	0.14
	2	165	0.38		2	206	0.38
	3	238	0.54		3	298	0.54
	4	290	0.66		4	364	0.67
	5	327	0.75		5	412	0.75
	7	374	0.86		7	473	0.86
	14	425	0.97		14	536	0.98
	21	434	0.99		21	545	1.00
	28	437	1.00		28	548	1.00
d_s14	1	73	0.14	d_s16	1	67	0.14
	2	191	0.38		2	175	0.38
	3	275	0.54		3	253	0.54
	4	336	0.66		4	308	0.66
	5	380	0.75		5	348	0.75

	7	436	0.86		7	399	0.86
	14	495	0.98		14	452	0.98
	21	504	1.00		21	461	0.99
	28	506	1.00		28	464	1.00

654



655

Fig. 21. Time-dependent evolution functions of: (a) restrained tensile stress; (b) restrained shrinkage strain.

656

657

$$\frac{\sigma_{ct,re}(t)}{\sigma_{ct,re,28}} = 1 - e^{-7.25\left(\frac{t}{28}\right)} \quad (35)$$

658

$$\frac{\varepsilon_{cs,re}(t)}{\varepsilon_{cs,re,28}} = 1 - e^{-7.25\left(\frac{t}{28}\right)} \quad (36)$$

659

The restraint degree ζ , defined as the ratio of the restrained tensile stress $\sigma_{ct,re}$ (analytical values) to the tensile strength f_{ct} at 28d under the standard curing condition, was proposed to characterize the degree to which the rebar contributed to reducing the first cracking strength for CA-UHPC. Similarly, the free degree ψ , expressed as the ratio of the restrained shrinkage strain $\varepsilon_{cs,re}$ (analytical values) to the free shrinkage strain ε_{cs} at 28d under the standard curing condition, was defined to quantify the effect of rebar on the free shrinkage development of CA-UHPC. The expressions of ζ and ψ are given in Eq.(37) and Eq.(38), respectively, and the calculated values are listed in Table 13.

667

$$\zeta = \frac{\sigma_{ct,re}}{f_{ct}} \quad (37)$$

668

$$\psi = \frac{\varepsilon_{cs,re}}{\varepsilon_{cs}} \quad (38)$$

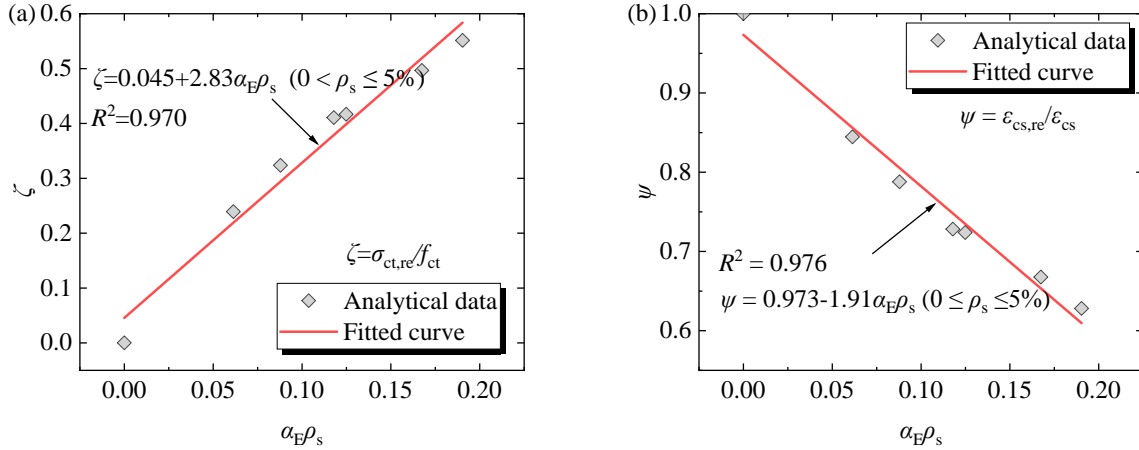
669

Table 13. Restraint degree ζ and free degree ψ of R-CA-UHPC members.

Rebar	$\alpha E \rho_s$	Tensile stress			Shrinkage strain		
		$\sigma_{ct,re}$ [MPa]	f_{ct} [MPa]	ζ	$\varepsilon_{cs,re} [\times 10^{-6}]$	$\varepsilon_{cs} [\times 10^{-6}]$	ψ
$d_s 10$	0.061	2.31	7.83	0.24	587	695	0.87
$2d_s 10$	0.125	3.24		0.42	503		0.72
$3d_s 10$	0.190	3.80		0.55	437		0.63

d_s12	0.088	2.75		0.32	548		0.79
d_s14	0.118	3.09		0.41	506		0.73
d_s16	0.167	4.50		0.50	464		0.67

670 The restraint degree ζ and free degree ψ are highly correlated with the axial stiffness
671 ratio $\alpha_E\rho_s$ (E_sA_s/E_cA_c) of rebar to concrete. The relation between ζ , ψ and $\alpha_E\rho_s$ were linearly
672 fitted, plotted in Fig.22, with a goodness-of-fit R^2 of up to 97%. The fitted expressions are
673 given in Eq.(39) and Eq.(40), respectively. It is worth noting that the applicable conditions of
674 these expressions are: (1) steel rebar reinforced CA-UHPC members under standard curing
675 for 28 days, and (2) corresponding reinforcement ratio $0 < \rho_s \leq 5\%$.



676 **Fig. 22.** Relation between axial tension stiffness ratio $\alpha_E\rho_s$ and (a) restraint degree ζ ; (b) free
677 degree ψ .

$$\zeta = 0.045 + 2.83\alpha_E\rho_s \quad (39)$$

$$\psi = 0.973 - 1.91\alpha_E\rho_s \quad (40)$$

680 Therefore, the first cracking strength f_{cr} and strain ε_{cr} of R-CA-UHPC members under the
681 standard curing for 28 days can be predicted based on the restraint degree ζ as follows, once
682 obtaining the tensile strength f_{ct} , the elastic modulus E_c , and the axial stiffness ratio of rebar to
683 CA-UHPC $\alpha_E\rho_s$.

$$f_{cr} = f_{ct}(1 - \zeta) \quad (41)$$

$$\varepsilon_{cr} = \frac{f_{cr}}{E_c} \quad (42)$$

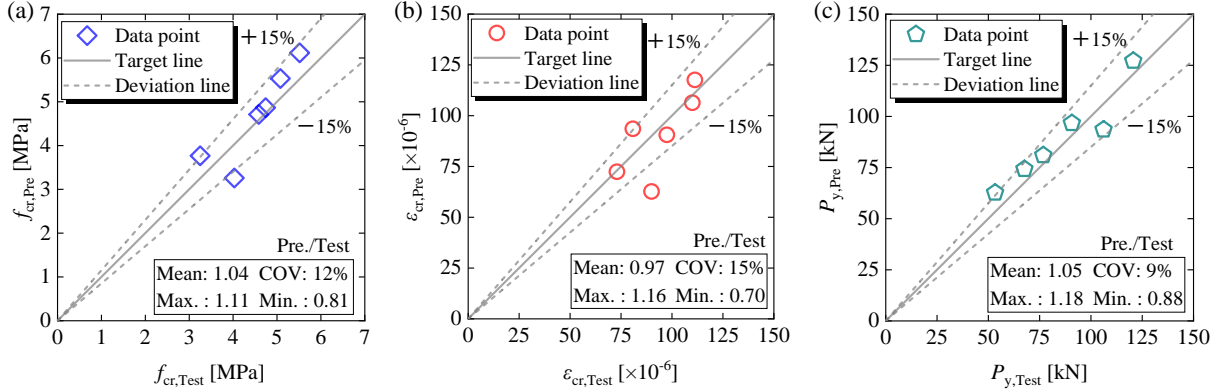
686 As observed in sec.4.3, the restrained shrinkage creep effect postponed rebar yield by the
687 restrained shrinkage strain $\varepsilon_{cr,re}$ which could be predicted by Eq.(38) and Eq.(40). The actual
688 strain of rebar at the average member strain ε reaching ε_{sy} was obtained by subtracting $\varepsilon_{cr,re}$
689 from ε_{sy} , as given in Eq.(43). Then, the corresponding yielding load (pseudo yielding) could
690 be predicted as expressed in in Eq.(44).

$$\varepsilon_{y1} = \varepsilon_{sy} - \varepsilon_{cr,re} = \varepsilon_{sy} - \psi\varepsilon_{cs} \quad (43)$$

$$P_y = P_{yc} + P_{ys} = A_c\sigma_{ct}(\varepsilon = \varepsilon_{sy} - \psi\varepsilon_{cs}) + A_s\sigma_s(\varepsilon = \varepsilon_{sy} - \psi\varepsilon_{cs}) \quad (44)$$

693 Fig.23 plots the comparison between prediction and test values for the first cracking

694 strength f_{cr} , the first cracking strain ε_{cr} , and the yielding load P_y . As shown, the prediction
 695 values were 1.04, 0.97, and 1.05 times the test values for f_{cr} , ε_{cr} , and P_y , respectively, and the
 696 corresponding coefficient of variation were 12%, 16%, and 9%, respectively. It indicated that
 697 the models established had a high accuracy exceeding 90% and could be used to predict these
 698 characteristic responses for R-CA-UHPC members.



699
 700 **Fig. 23.** Comparison between prediction and test values: (a) first cracking strength f_{cr} ; (b)
 701 first cracking strain ε_{cr} ; (c) yielding load P_y .

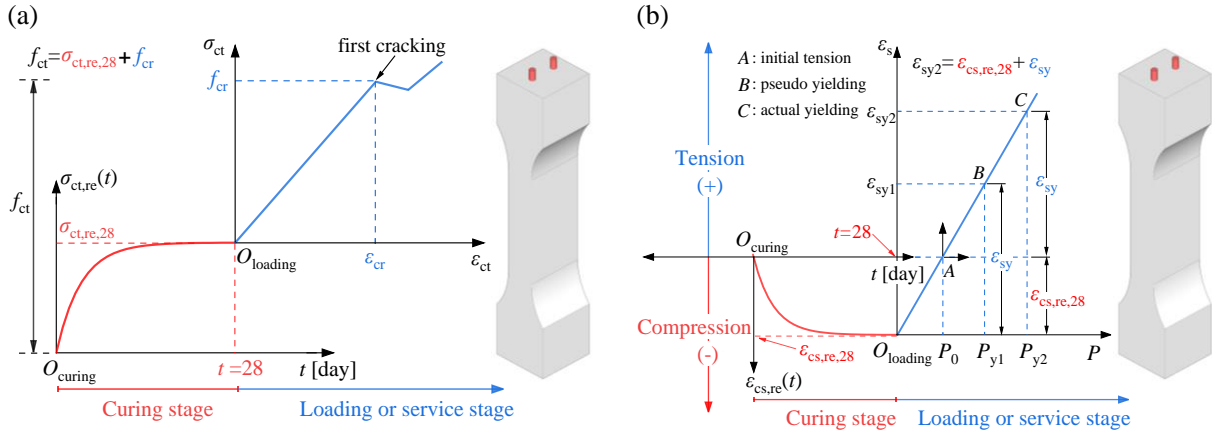
702 *5.4 Structural design suggestions*

703 In general, the tensile capacity of NC elements is neglected in R-NC structures because
 704 of the limited tensile strength of NC material. UHPC and CA-UHPC present significantly
 705 improved tensile strength through the enhanced dense microstructures and the addition of
 706 steel fibers, which is promising for more resilient structures. The tensile behavior of R-CA-
 707 UHPC members is not just a simple superposition of the tensile properties of steel bars and
 708 CA-UHPC, but the relatively high shrinkage of CA-UHPC and the interaction between rebar
 709 and CA-UHPC must be considered in structural design to ensure the safety at the
 710 serviceability limit state as well as the ultimate limit state.

711 The influence of the restrained shrinkage and related creep-induced stress relaxation
 712 effects on the tensile stress development of CA-UHPC and the tensile strain development of
 713 rebar for the R-CA-UHPC members are plotted in Fig.24. As shown, the restrained tensile
 714 stress for CA-UHPC developed at the curing stage accounts for a considerable proportion of
 715 the tensile strength of CA-UHPC material, causing the premature cracking of the member at
 716 service stage. The development function of the restrained tensile stress at the curing stage is
 717 suggested using Eq.(35), and the resulting first cracking values are suggested to predict
 718 according to Eq.(39)~(42).

719 As shown in Fig.24(b), the interaction between rebar and concrete leads to compression
 720 in the rebar at the curing stage. The evolution of the compressive strain due to the restrained
 721 shrinkage, can be quantified based on Eq.(36). At the service stage under the tensile load, the
 722 rebar firstly sustains compression and has to zero the compression until reaching point A and
 723 starts bearing tension. Point B, marked as the pseudo yielding point, is determined by the
 724 average member strain reaching the yielding strain of rebar ε_{sy} , while the actual strain of rebar
 725 merely arrives $\varepsilon_{sy}-\varepsilon_{cr,re,28}$. By comparison, point C is the actual yielding point for the rebar,

726 where the average member strain and the rebar strain are $\epsilon_{sy} + \epsilon_{cr, re, 28}$ and ϵ_{sy} , respectively. The
 727 final compressive strain or the restrained shrinkage strain $\epsilon_{cr, re, 28}$ is recommended to be
 728 predicted according to Eq.(38) and Eq.(40). Accordingly, the corresponding pseudo-yielding
 729 and actual-yielding loads for R-CA-UHPC members are to be determined based on the
 730 superposition of the tensile loads carried by CA-UHPC and rebar, respectively.



731
 732 **Fig. 24.** Stress and strain development of R-CA-UHPC members at different stages: (a)
 733 tensile stress of CA-UHPC; (b) strain of rebar.

734 6. Conclusions

735 Based on the above investigations, the main conclusions are:

- 736 (1) The axial tensile response of R-NC members consists of the linear-elastic phase, the
 737 stabilized cracking phase, and the yielding phase accompanied by the longitudinal
 738 splitting cracking. The axial tensile response of R-CA-UHPC members is
 739 decomposed into the linear-elastic, the stabilized multi-cracking, the rebar yielding
 740 (localized cracking in CA-UHPC), and fracture phases. The excellent bond properties
 741 between rebar and CA-UHPC prevent the emergence of splitting cracks, but intensify
 742 the crack localization for CA-UHPC and strain concentration for rebar, leading to the
 743 ultimate fracture of rebar.
- 744 (2) The restrained shrinkage creep effect at the curing stage induces a restrained tensile
 745 stress in CA-UHPC and a restrained shrinkage compressive strain in rebar, which
 746 reduces the first cracking of CA-UHPC and delays the yield of rebar. The restrained
 747 tensile stress increases with the increase of the axial stiffness ratio of rebar to CA-
 748 UHPC, while the restrained shrinkage strain exhibits an opposite trend.
- 749 (3) Based on the test results of this study and literature, the development model of elastic
 750 modulus for CA-UHPC at early age has been developed. The development models of
 751 autogenous shrinkage and tensile creep for CA-UHPC at early age have been
 752 established in the light of data from the literature. Based on these age-dependent
 753 models, the restrained tensile stress and shrinkage strain have been quantified
 754 according to Dischinger's differential equation, and have demonstrated a high
 755 accuracy of up to 96% by comparing with the test results.
- 756 (4) The concepts of restraint degree and free degree were proposed and fitted with the
 757 axial stiffness ratio of rebar to CA-UHPC, to determine the restrained effect of rebar

758 on free shrinkage of CA-UHPC. On this basis, prediction models of the first cracking
759 stress, the first cracking strain, and the yielding load for R-CA-UHPC members
760 under axial tension were established with a prediction accuracy of exceeding 90%.

761 **7. Acknowledgements**

762 The financial support provided by Fujian Transportation Science and Technology Project
763 (Grant NO.202126) is greatly appreciated by the authors. The first author also acknowledges
764 the financial support of the China Scholarship Council (Grant NO. 202006260216).

765 **References**

- 766 [1] B. Graybeal, E. Brühwiler, B.-S. Kim, F. Toutlemonde, Y.L. Voo, A. Zaghi, International
767 perspective on UHPC in bridge engineering, *Journal of Bridge Engineering* 25 (2020)
768 04020094.
- 769 [2] K. Habel, E. Denarié, E. Brühwiler, Experimental investigation of composite ultra-high-
770 performance fiber-reinforced concrete and conventional concrete members, *ACI*
771 *Structural Journal* 104 (2007) 93.
- 772 [3] H. Martín-Sanz, B. Herraiz, E. Brühwiler, E. Chatzi, Shear-bending failure modeling of
773 concrete ribbed slabs strengthened with UHPFRC, *Engineering Structures* 222 (2020)
774 110846.
- 775 [4] Y. Zhang, X. Li, Y. Zhu, X. Shao, Experimental study on flexural behavior of damaged
776 reinforced concrete (RC) beam strengthened by toughness-improved ultra-high
777 performance concrete (UHPC) layer, *Composites Part B: Engineering* 186 (2020)
778 107834.
- 779 [5] Y. Zhang, Y. Zhu, M. Yeseta, D. Meng, X. Shao, Q. Dang, G. Chen, Flexural behaviors
780 and capacity prediction on damaged reinforcement concrete (RC) bridge deck
781 strengthened by ultra-high performance concrete (UHPC) layer, *Construction and*
782 *Building Materials* 215 (2019) 347–359.
- 783 [6] P. Buitelaar, R. Braam, N. Kaptijn, Reinforced High Performance Concrete Overlay
784 System for Rehabilitation and Strengthening of Orthotropic Steel bridge decks, in: 2004
785 Orthotropic Bridge Conference, 2004.
- 786 [7] J. Cao, X. Shao, Z. Zhang, H. Zhao, Retrofit of an orthotropic steel deck with compact
787 reinforced reactive powder concrete, *Structure and Infrastructure Engineering* 12 (2016)
788 411–429. <https://doi.org/10.1080/15732479.2015.1019894>.
- 789 [8] S. Wang, Z. Ke, Y. Gao, Y. Zhang, Long-Term In Situ Performance Investigation of
790 Orthotropic Steel Bridge Deck Strengthened by SPS and RPC Solutions, *J. Bridge Eng.*
791 24 (2019) 04019054. [https://doi.org/10.1061/\(ASCE\)BE.1943-5592.0001421](https://doi.org/10.1061/(ASCE)BE.1943-5592.0001421).
- 792 [9] D. Wang, C. Shi, Z. Wu, J. Xiao, Z. Huang, Z. Fang, A review on ultra high performance
793 concrete: Part II. Hydration, microstructure and properties, *Construction and Building*
794 *Materials* 96 (2015) 368–377.
- 795 [10] L. Yang, C. Shi, Z. Wu, Mitigation techniques for autogenous shrinkage of ultra-high-
796 performance concrete—A review, *Composites Part B: Engineering* 178 (2019) 107456.

- 797 [11] J. Liu, F. Han, G. Cui, Q. Zhang, J. Lv, L. Zhang, Z. Yang, Combined effect of coarse
798 aggregate and fiber on tensile behavior of ultra-high performance concrete, *Construction*
799 *and Building Materials* 121 (2016) 310–318.
800 <https://doi.org/10.1016/j.conbuildmat.2016.05.039>.
- 801 [12] C. Li, B. Chen, J. Wei, Shrinkage and mechanical properties of UHPC with coarse
802 aggregate, *Journal of Traffic and Transportation Engineering* 19 (2019) 11–20.
- 803 [13] Z. Shi, Q. Su, F. Kavoura, M. Veljkovic, Uniaxial tensile response and tensile
804 constitutive model of ultra-high performance concrete containing coarse aggregate (CA-
805 UHPC), *Cement and Concrete Composites* 136 (2023) 104878.
806 <https://doi.org/10.1016/j.cemconcomp.2022.104878>.
- 807 [14] L. Li, L. Xu, Y. Zeng, K. Cui, Y. Chi, L. Huang, Understanding the role of coarse
808 aggregate on tensile fatigue behaviors of ultra-high performance concrete, *Cement and*
809 *Concrete Composites* 139 (2023) 105069.
- 810 [15] J. Cheng, Study on flexural fatigue performance of ultra high performance concrete with
811 coarse aggregate, Master's dissertation, Southeast University, 2018.
- 812 [16] J. Qi, Y. Bao, J. Wang, L. Li, W. Li, Flexural behavior of an innovative dovetail UHPC
813 joint in composite bridges under negative bending moment, *Engineering Structures* 200
814 (2019) 109716.
- 815 [17] Z. Liu, M. Alsomiri, M. Li, X. Chen, J. Meng, Experimental investigation on the flexural
816 behavior of coarse aggregate reactive powder concrete (CA-RPC) bridge deck,
817 *Engineering Structures* 271 (2022) 114951.
- 818 [18] Y. Wang, X. Shao, J. Cao, Experimental study on basic performances of reinforced
819 UHPC bridge deck with coarse aggregates, *Journal of Bridge Engineering* 24 (2019)
820 04019119.
- 821 [19] K. Lu, Q. Xu, L. Du, J. Wang, Y. Yao, Fatigue performance of prefabricated coarse
822 aggregate ultrahigh-performance concrete deck subjected to negative bending moment,
823 *Engineering Structures* 274 (2023) 115098.
- 824 [20] J. Jungwirth, A. Muttoni, Structural Behavior of Tension Members in UHPC. École
825 Polytechnique Fédérale de Lausanne, IS-Beton, (2004).
- 826 [21] T. Makita, E. Brühwiler, Tensile fatigue behaviour of Ultra-High Performance Fibre
827 Reinforced Concrete combined with steel rebars (R-UHPFRC), *International Journal of*
828 *Fatigue* 59 (2014) 145–152.
- 829 [22] C.-C. Hung, H.-S. Lee, S.N. Chan, Tension-stiffening effect in steel-reinforced UHPC
830 composites: Constitutive model and effects of steel fibers, loading patterns, and rebar
831 sizes, *Composites Part B: Engineering* 158 (2019) 269–278.
832 <https://doi.org/10.1016/j.compositesb.2018.09.091>.
- 833 [23] H. Yuan, Theoretical analysis and experimental research on tensile performance of
834 reinforced reactive powder concrete, Doctoral thesis, Beijing Jiaotong University, 2009.
- 835 [24] Z. Zhang, X.-D. Shao, P. Zhu, Direct tensile behaviors of steel-bar reinforced ultra-high
836 performance fiber reinforced concrete: Effects of steel fibers and steel rebars,
837 *Construction and Building Materials* 243 (2020) 118054.
- 838 [25] M. Qiu, Y. Zhang, S. Qu, Y. Zhu, X. Shao, Effect of reinforcement ratio, fiber

- 839 orientation, and fiber chemical treatment on the direct tension behavior of rebar-
840 reinforced UHPC, *Construction and Building Materials* 256 (2020) 119311.
841 <https://doi.org/10.1016/j.conbuildmat.2020.119311>.
- 842 [26] C. Bian, J.-Y. Wang, Mechanical and damage mechanisms of reinforced ultra high
843 performance concrete under tensile loading, *Construction and Building Materials* 226
844 (2019) 259–279. <https://doi.org/10.1016/j.conbuildmat.2019.07.162>.
- 845 [27] J.-Y. Guo, J.-Y. Wang, C. Bian, Synergistic tensile response of reinforced ultra high
846 performance concrete with low fiber contents, *Case Studies in Construction Materials* 17
847 (2022) e01629.
- 848 [28] C. Bian, J. Guo, J. Wang, J. Xiao, Nominal tensile strength reduction and its mechanism
849 of ultra-high performance concrete with steel bar reinforcements, *Journal of Building
850 Engineering* 65 (2023) 105778.
- 851 [29] M. Roy, C. Hollmann, K. Wille, Influence of fiber volume fraction and fiber orientation
852 on the uniaxial tensile behavior of rebar-reinforced ultra-high performance concrete,
853 *Fibers* 7 (2019) 67.
- 854 [30] M. Khorami, J. Navarro-Gregori, P. Serna, Tensile behaviour of reinforced UHPFRC
855 elements under serviceability conditions, *Materials and Structures* 54 (2021) 1–17.
- 856 [31] J. Yu, T. Shi, J. Yu, Z. Xie, K. Yu, Experimental study of tensile properties of composite
857 system of high performance concrete and reinforcements, *Journal of Tongji University
858 (Natural Science)* 49 (2021) 825–833.
- 859 [32] K. Fields, P.H. Bischoff, Tension stiffening and cracking of high-strength reinforced
860 concrete tension members, *ACI Structural Journal* 101 (2004) 447–456.
- 861 [33] S.A. Altoubat, D.A. Lange, Creep, shrinkage, and cracking of restrained concrete at early
862 age, *ACI Materials Journal* 98 (2001) 323–331.
- 863 [34] Dalian University of Technology, Standard test methods for fiber reinforced concrete,
864 China Planning Press, Beijing, China, 2010.
- 865 [35] SAC/TC183, GB / T228-2002 Metallic materials-Tensile testing at ambient temperature,
866 General Administration of Quality Supervision, Inspection and Quarantine of the
867 People’s Republic of China, Beijing, China, 2002.
- 868 [36] D.-Y. Yoo, N. Banthia, Y.-S. Yoon, Effectiveness of shrinkage-reducing admixture in
869 reducing autogenous shrinkage stress of ultra-high-performance fiber-reinforced
870 concrete, *Cement and Concrete Composites* 64 (2015) 27–36.
- 871 [37] H. Rüsçh, D. Jungwirth, H.K. Hilsdorf, Creep and shrinkage: their effect on the behavior
872 of concrete structures, Springer-Verlag, New York, U.S.A., 2012.
- 873 [38] B.A. Graybeal, Compressive Behavior of Ultra-High-Performance Fiber-Reinforced
874 Concrete, *ACI Materials Journal* 104 (2007) 146–152. <https://doi.org/10.14359/18577>.
- 875 [39] D.-Y. Yoo, S. Kim, M.-J. Kim, Comparative shrinkage behavior of ultra-high-
876 performance fiber-reinforced concrete under ambient and heat curing conditions,
877 *Construction and Building Materials* 162 (2018) 406–419.
878 <https://doi.org/10.1016/j.conbuildmat.2017.12.029>.
- 879 [40] European Committee for Standardization, EN 1992-1-1: Eurocode 2: Design of concrete
880 structures - Part 1-1: General rules and rules for buildings, Brussels, Belgium, 2004.

881 [41] SIA, SIA 2052 Recommendation: Ultra-High Performance Fibre Reinforced Cement-
882 based Composites (UHPFRC) Construction material, dimensioning und application,
883 Zurich, Switzerland, 2016.
884

Declaration of interests

The authors declare that they have no known competing financial interests or personal relationships that could have appeared to influence the work reported in this paper.

The authors declare the following financial interests/personal relationships which may be considered as potential competing interests: